Respiratory Alkalosis Provokes Spike-Wave Discharges in Seizure-Prone Rats

Author names and affiliations

Kathryn A. Salvati[1,2*], George M.P.R. Souza[1], Adam C. Lu[1,2], Matthew L. Ritger[1,2], Patrice G. Guyenet[1], Stephen B. Abbott[1], Mark P. Beenhakker[1*]

[1] Department of Pharmacology, University of Virginia, Charlottesville, VA, USA.

[2] Neuroscience Graduate Program, University of Virginia, Charlottesville, VA, USA.

*Co-corresponding authors

Abstract

Hyperventilation reliably provokes seizures in patients diagnosed with absence epilepsy. Despite this predictable patient response, the mechanisms that enable hyperventilation to powerfully activate absence seizure-generating circuits remain entirely unknown. Using the WAG/Rij rat, an established rodent model of absence epilepsy, we demonstrate that absence seizures are highly sensitive to arterial carbon dioxide, suggesting that seizure-generating circuits are sensitive to pH. Moreover, hyperventilation consistently activated neurons within the intralaminar nuclei of the thalamus, a structure implicated in seizure generation. We show that intralaminar thalamus also contains pH-sensitive neurons. Collectively, these observations suggest that hyperventilation activates pH-sensitive neurons of the intralaminar nuclei to provoke absence seizures.

Introduction

Epilepsy is a common neurological disorder characterized by recurrent and spontaneous seizures. Yet, accumulating evidence indicates that seizures are not necessarily unpredictable events (Amengual-Gual et al., 2019; Bartolini & Sander, 2019; Baud et al., 2018; Ferlisi & Shorvon, 2014). Several factors affect seizure occurrence, including metabolism (Lusardi et al., 2015; Masino et al., 2012; Masino & Rho, 2012, 2019), sleep (Bazil, 2019; Fountain et al., 1998; Malow et al., 1999; Nobili et al., 2001), catamenia (Herzog & Frye, 2014; Joshi & Kapur, 2019; Reddy et al., 2001), light (Padmanaban et al., 2019) and circadian rhythm (Amengual-Gual et al., 2019; Debski et al., 2020; Smyk & van Luijtelaar, 2020; Stirling et al., 2021). In extreme cases, stimuli immediately provoke seizures, a condition known as *reflex epilepsy* (Kasteleijn-Nolst Trenité, 2012; Koepp et al., 2016). The mechanisms that render certain seizure-generating networks susceptible to external factors remain unknown.

A highly reliable seizure trigger associated with childhood absence epilepsy is hyperventilation. Between 87-100% of all children diagnosed with the common *Genetic Generalized Epilepsy* produce spike-wave seizures upon voluntary hyperventilation (Hughes,

2009; Ma et al., 2011; Sadleir et al., 2009). Indeed, hyperventilation serves as a powerful tool for diagnosing this childhood epilepsy (Adams & Lueders, 1981; Holowach et al., 1962; Sadleir et al., 2006; Watemberg et al., 2015). Remarkably, as no single genetic etiology drives absence epilepsy (Chen et al., 2013; Crunelli & Leresche, 2002; Helbig, 2015; Koeleman, 2018; Robinson et al., 2002; Xie et al., 2019), hyperventilation appears to recruit fundamental seizure-generating mechanisms shared by virtually all patients.

Exhalation of CO_2 during hyperventilation causes hypocapnia, a state of decreased arterial CO_2 partial pressure ($PaCO_2$), and respiratory alkalosis, a state of elevated arterial pH (Laffey & Kavanagh, 2002). Hyperventilation also causes rapid arterial vasoconstriction (Raichle & Plum, 1972) and increased cardiac output (Donevan et al., 1962). Recent work demonstrates that inspiration of 5% CO_2 blunts hyperventilation-provoked spike-wave seizures in humans (Yang et al., 2014). Collectively, these observations suggest that respiratory alkalosis serves as the primary trigger for hyperventilation-provoked absence seizures.

Spike-wave seizures associated with absence epilepsy arise from hypersynchronous neural activity patterns within interconnected circuits between the thalamus and the cortex (Avoli, 2012; Beenhakker & Huguenard, 2009; Huguenard & McCormick, 2007; McCafferty et al., 2018; McCormick & Contreras, 2001; Meeren et al., 2002). The crux of the prevailing model describing absence seizure generation includes an initiating bout of synchronous activity within the somatosensory cortex that recruits rhythmically active circuits in the thalamus (Meeren et al., 2002; Sarrigiannis et al., 2018). With widespread connectivity to the cortex, the thalamus then rapidly generalizes spike-wave seizures to other brain structures. The extent to which thalamocortical circuits respond to shifts in pH during hyperventilation-induced respiratory alkalosis is unknown.

Herein, we test the hypothesis that respiratory alkalosis regulates the occurrence of spike-wave seizures. We demonstrate that hyperventilation-provoked absence seizures observed in humans can be mimicked in an established rodent model, the WAG/Rij rat (Coenen, 2003;

Coenen et al., 1992; Russo et al., 2016; van Luijtelaar & Coenen, 1986). We first show that hyperventilation induced with hypoxia reliably evokes respiratory alkalosis and increases spike-wave seizure count in the WAG/Rij rat. When supplemented with 5% CO_2 to offset respiratory alkalosis, hypoxia did not increase spike-wave seizure count. Moreover, hypercapnia alone (high $PaCO_2$) reduced spike-wave seizure count despite a robust increase in respiration rate. We also show that optogenetic stimulation of brainstem respiratory centers to produce respiratory alkalosis during normoxia induces CO_2-sensitive spike-wave seizures. Collectively, these results identify respiratory alkalosis as the primary seizure trigger in absence epilepsy following hyperventilation. Finally, we show that structures of the intralaminar thalamic nuclei are both (1) activated during respiratory alkalosis, and (2) pH-sensitive. Thus, our data demonstrate that respiratory alkalosis provokes spike-wave seizures and shine a spotlight on the poorly understood intralaminar thalamus in the pathophysiology of spike-wave seizures.

Results

Hypoxia triggers spike-wave seizures in the WAG/Rij rat

We first set out to determine if an accepted rat model of absence epilepsy, the WAG/Rij rat, recapitulates hyperventilation-provoked absence seizures, as observed in humans. We combined whole-body plethysmography and electrocorticography/electromyography (ECoG/EMG) recordings in awake WAG/Rij rats to assess respiration and spike-wave seizure occurrence while exposing animals to different gas mixtures of O_2, CO_2 and N_2 (Figure 1A,B). We only considered spike-wave seizures that persisted for a minimum of two seconds and occurred concomitantly with behavioral arrest in the animal. Spike-wave seizures are distinguishable from non-REM sleep based on the appearance of 5-8 Hz frequency harmonics in the power spectrogram (see Figure 1B, *expanded trace*).

We first compared respiration and ECoG/EMG activity in rats exposed to atmospheric conditions (i.e., normoxia: 21% O_2; 0% CO_2; 79% N_2) and hypoxia (10% O_2; 0% CO_2; 90% N_2).

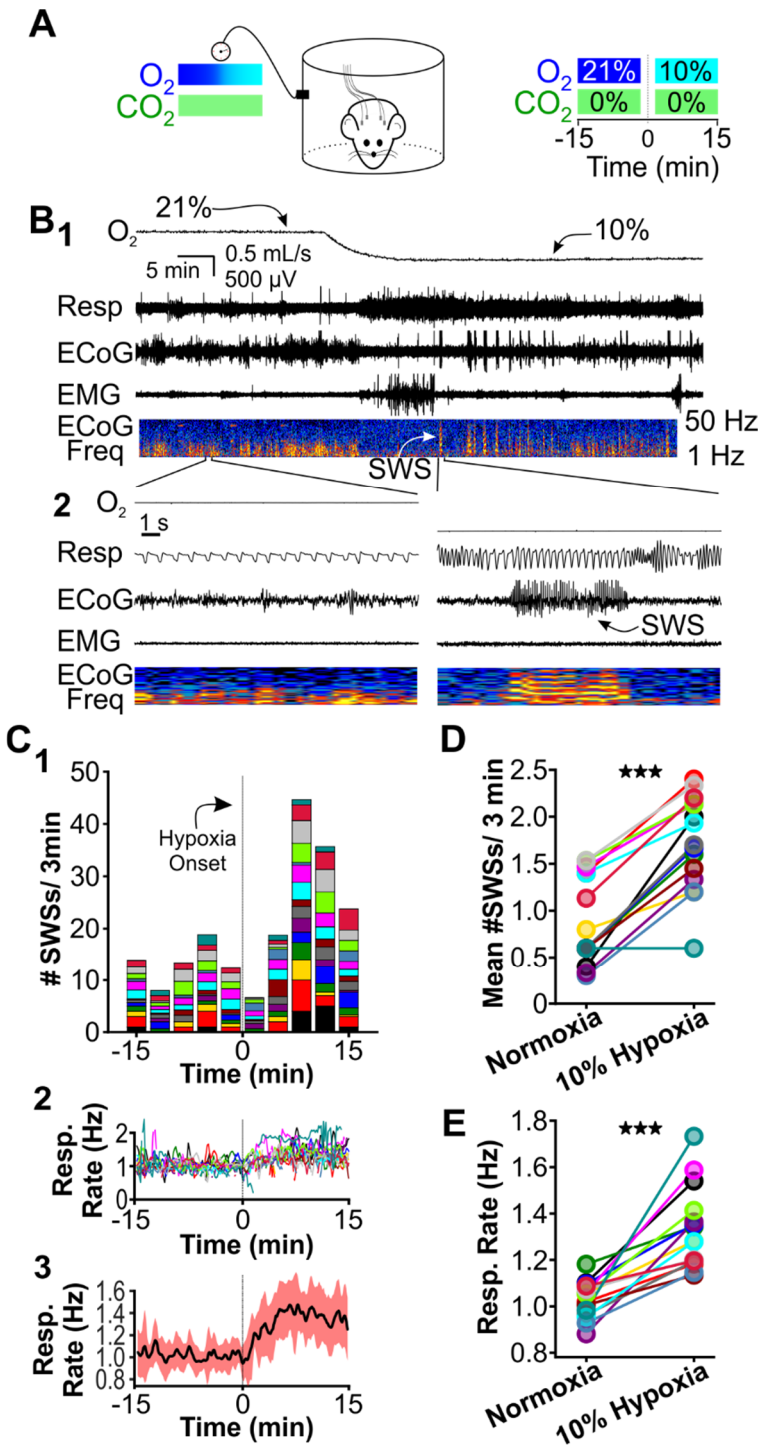

Figure 1. Hypoxia provokes hyperventilation-associated spike-wave seizures in WAG/Rij rats.

(A) Experiment Paradigm. *Left:* Plethysmography chambers recorded ventilation and ECoG/EMG signals in rats exposed to normoxia (i.e., 21% O_2) and hypoxia (i.e., 10% O_2). *Right:* Example gas exchange protocol used to generate the peristimulus time histogram in panel C. Spike-wave seizure count was measured during the 15 minutes before and after gas exchange at t = 0 min. **(B)** Representative recordings during transition from normoxia to

hypoxia. (1) From top to bottom: chamber O_2, respiration, ECoG, EMG, and ECoG power spectrogram. White arrow points to spike-wave seizure. (2) *Bottom:* expanded view B1. Spectrogram reveals 5-8 Hz frequency harmonics associated with spike-wave seizures. **(C)** Spike-wave seizure (SWS) and respiration quantification. (1) Stacked histogram illustrating spike-wave seizure count for each animal before and after the onset of hypoxia; each color is a different rat. Arrow points to gas exchange at t = 0 min. (2) Corresponding respiratory rate for each animal shown in panel C1. (3) Mean respiratory rate for all animals. **(D)** Mean spike-wave seizure count per bin and **(E)** respiratory rate before and after gas exchange. See **Tables 1 & 2** for detailed statistics. ***p < 0.001.

Hypoxia reliably stimulates rapid breathing, blood alkalosis and hypocapnia in rats (Basting et al., 2015; Souza et al., 2019). We cycled rats between 40-minute epochs of normoxia and 20-minute epochs of hypoxia. O_2 levels were measured from the outflow of the plethysmography chamber for confirmation of gas exchange (Figure 1B, *top*). Hypoxia evoked a robust increase in respiratory rate (Figure 1B, *expanded*) and reliably provoked seizures. A peristimulus time histogram (PSTH) aligned to the onset of gas exchange shows spike-wave seizure counts during the 15 minutes immediately before and during hypoxia (Figure 1C1); the PSTH shows the contribution of each rat in stacked histogram format. Respiratory rates confirmed that hypoxia increased ventilation (Figure 1C2,3). To quantify the effect of hypoxia on seizures, we calculated the mean spike-wave seizure count across all bins for each rat. Relative to normoxia, spike-wave seizure count during hypoxia was nearly 2-fold higher ($p = 4.5 \times 10^{-7}$, n = 15; Fig. 1D) and respiratory rate increased by 30% ($p = 1.6 \times 10^{-5}$, n = 15; Fig. 1E).

Recent work shows that spike-wave seizures commonly occur in several rat strains, including those that are generally not considered epileptic (Taylor et al., 2017, 2019). While between 62% (Vergnes et al., 1982) and 84% (Robinson & Gilmore, 1980) of Wistar rats do not have seizures, we nonetheless tested whether hypoxia can unmask seizure-generating potential in this strain, as Wistar and WAG/Rij rats share the same genetic background (Festing, 1979). In normoxia, seizures were absent in all four Wistar rats we tested, consistent with the infrequent spike-wave seizure occurrence reported for this strain. Relative to normoxia in Wistar rats, hypoxia induced hyperventilation, hypocapnia and blood alkalization but did not provoke spike-

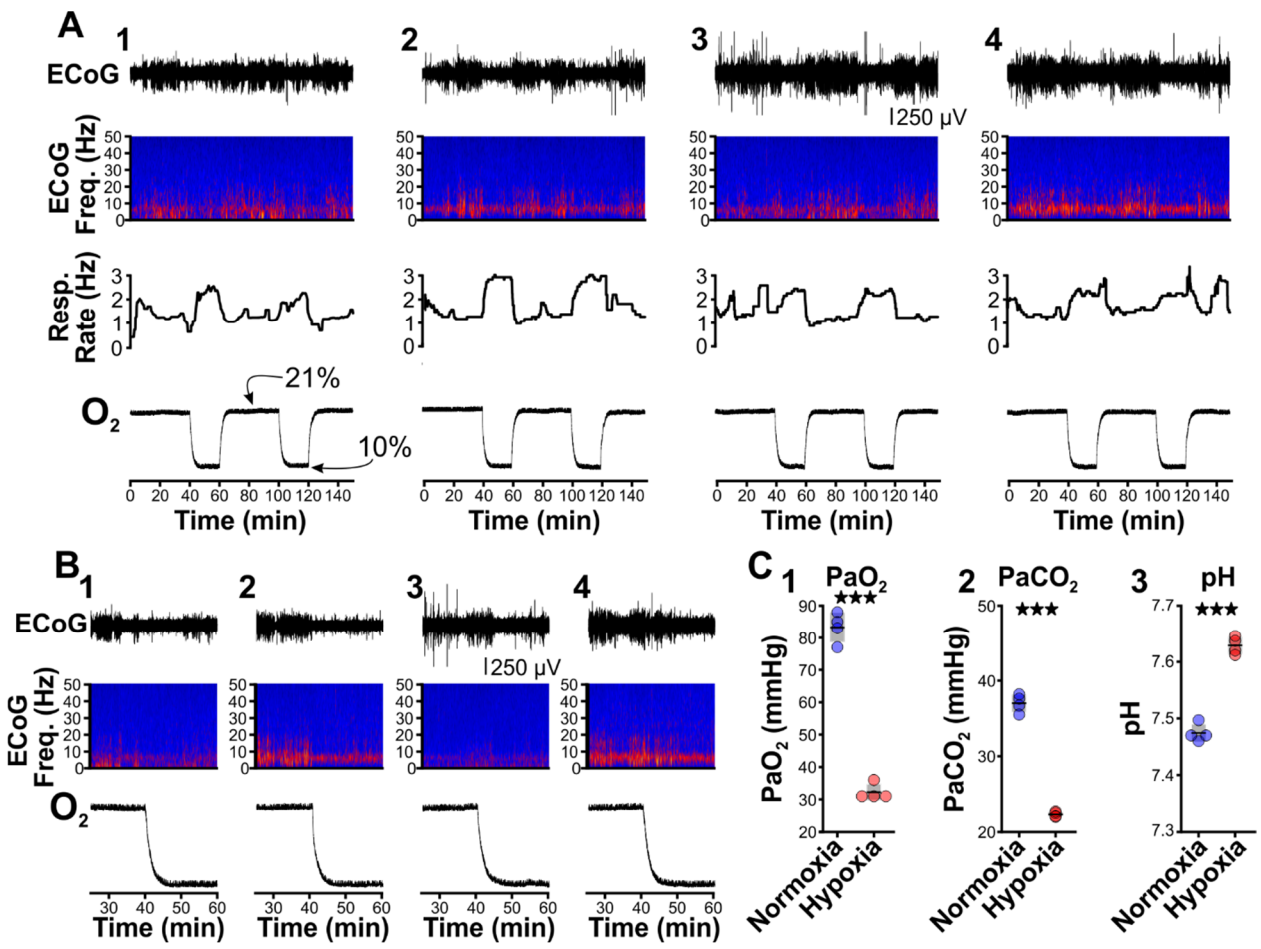

Figure 2. Hypoxia does not provoke hyperventilation-associated spike-wave seizures in Wistar rats. (A) Plethysmography chambers recorded ventilation and ECoG/EMG signals in four Wistar rats exposed to normoxia (i.e., 21% O_2) and hypoxia (i.e., 10% O_2). Panels 1-4 include responses from four Wistar rats, respectively, and show from top to bottom: ECoG, ECoG power spectrogram, respiratory rate, and chamber O_2. During the 2.5-hour recording session, rats were challenged twice with hypoxia. No spike-wave seizures were observed during either normoxia or hypoxia. **(B)** Expanded views of the first transition from normoxia to hypoxia shown in panel A. Increased low frequency power during normoxia in some rats (e.g., panel B2) represents sleep. Hypoxia in Wistar rats generally increased arousal. **(C)** Arterial measurements in the same rats show that hypoxia challenges produced a predictable drop in arterial (1) O_2 and (2) CO_2, as well as (3) alkalosis. See **Table 3** for detailed statistics. ***p < 0.001.

194 wave seizures (Figure 2; see Table 3). Instead, hypoxia primarily triggered arousal in Wistar rats,
195 as revealed in EEG spectrograms by the reduction in sleep-related frequencies. Therefore, we
196 hypothesize that hypoxia-provoked spike-wave seizures are unique to seizure-prone rodent
197 models, just as hyperventilation does not provoke absence seizures in otherwise healthy humans.
198
199 *CO_2 suppresses spike-wave seizures*
200 Hyperventilation promotes hypocapnia, a state of low $PaCO_2$. As dissolved CO_2 is acidic,
201 hyperventilation-triggered hypocapnia is also associated with respiratory alkalosis. To test the
202 hypothesis that hypocapnia specifically provokes seizures, we next determined whether
203 supplemental CO_2 (5%) blunts the spike-wave seizure-provoking effects of hypoxia. We
204 performed ECoG/plethysmography experiments as before but alternated between two test trials:
205 hypoxia and hypoxia/hypercapnia (10% O_2, 5% CO_2; 85% N_2). Test trials were interleaved with
206 40-minute periods of normoxia to allow blood gases to return to baseline levels (Figure 3A). As
207 before, hypoxia increased spike-wave seizure count by nearly 2-fold ($p = 1.76 \times 10^{-6}$, n = 9; Figure
208 3B1, C) and increased respiratory rate by 27% ($p = 6.59 \times 10^{-4}$, n = 9; Figure 3B3, D). In the same
209 rats, supplementing hypoxia with 5% CO_2 suppressed the spike-wave seizure response insofar
210 that hypoxia/hypercapnia did not change spike-wave seizure count relative to normoxia (p = 0.18,
211 n = 9; Figures 3E1 and 3F) despite a predictable and robust elevation in respiratory rate ($p = 2.71$
212 $\times 10^{-4}$, n = 9; Figures 3E2, 3 and 3G).
213 In a separate cohort of rats, we collected arterial blood samples to measure blood $PaCO_2$,
214 PaO_2 and pH during normoxia, hypoxia and hypoxia/hypercapnia (see Table 4). We observed a
215 considerable change in PaO_2 [$F(1.056, 5.281) = 406.4$, $p = 3.0 \times 10^{-6}$], $PaCO_2$ [$F(1.641, 8.203)$
216 $= 338.9$, $p = 1.9 \times 10^{-8}$] and pH [$F(1.938, 9.688) = 606$, $p = 7.2 \times 10^{-11}$] values among the three
217 conditions. Hypoxia decreased $PaCO_2$ ($p = 2.1 \times 10^{-6}$; n = 6; Figure 3H2) and concomitantly
218 alkalized the blood ($p = 7.0 \times 10^{-6}$, n = 6; Figure 3H3). We also observed a decrease in PaO_2 ($p =$
219 6.0×10^{-6}; n = 6; Figure 3H1). Supplemental CO_2 returned blood pH (p = 0.008, n = 6; Figure 3H3)

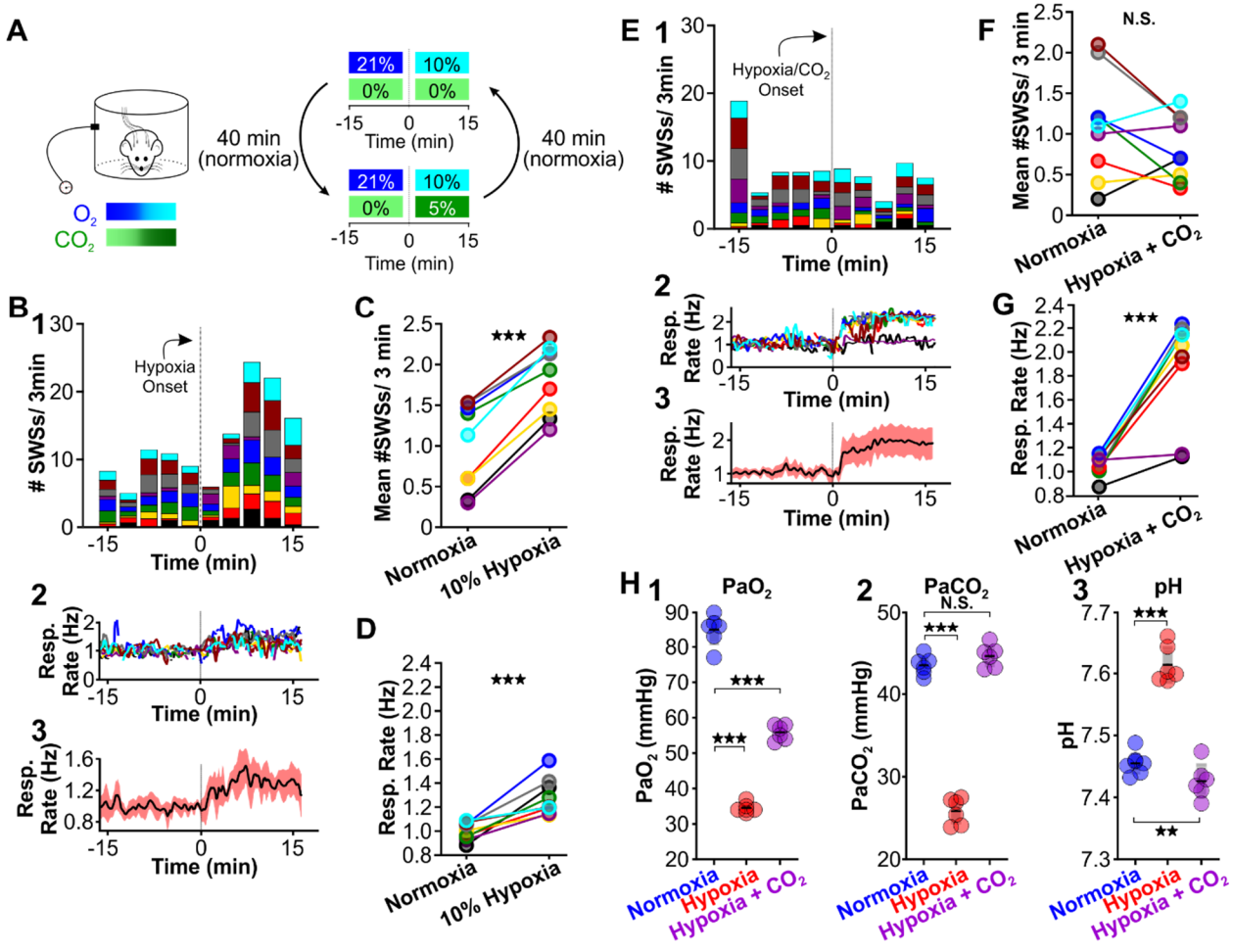

Figure 3. Supplemental CO_2 suppresses hypoxia-provoked spike-wave seizures.
(A) Experimental approach. Plethysmography chambers recorded ventilation and ECoG/EMG signals in WAG/Rij rats exposed to normoxia (i.e., 21% O_2) and then alternately challenged with hypoxia (i.e., 10% O_2) or hypoxia + CO_2, (i.e., 10% O_2, 5% CO_2). **(B-D)** Hypoxia challenge. **(B)** Spike-wave seizure (SWS) and respiration quantification. (1) Stacked histogram illustrating spike-wave seizure count for each animal before and after the onset of hypoxia. (2) Corresponding respiratory rate for each animal shown in panel B1. (3) Mean respiratory rate for all animals. **(C)** Mean spike-wave seizure count per bin and **(D)** respiratory rate before and after hypoxia exchange. **(E-G)** Hypoxia + CO_2 challenge. **(E)** SWS and respiration quantification. (1) Stacked histogram illustrating spike-wave seizure count for each animal before and after the onset of hypoxia + CO_2. (2) Corresponding respiratory rate for each animal shown in panel E1. (3) Mean respiratory rate for all animals. **(F)** Mean spike-wave seizure count per bin and **(G)** respiratory rate before after hypoxia + CO_2 exchange. **(H)** Arterial measurements in the same rats show that hypoxia produced a predictable drop in arterial (1) O_2 and (2) CO_2, as well as (3) respiratory alkalosis (as in Wistar rats). Supplementing the chamber with 5% CO_2 normalizes arterial CO_2 and pH. Elevated arterial O_2 during hypoxia + CO_2 relative to hypoxia reflects a powerful inhalation response during the former condition (c.f., panels D and G). See **Tables 1, 2 and 4** for detailed statistics. **p<0.01, ***p < 0.001.

and PaCO2 ($p = 0.42$, $n = 6$; Figure 3H2) to normoxia levels. However, heightened respiratory rate in supplemental CO_2 raised PaO_2 ($p = 00013$, $n = 6$; Figure 3H1). Collectively, these data support the hypothesis that blood pH powerfully regulates spike-wave seizure activity.

Next, we tested whether supplementing normoxia with 5% CO_2 is sufficient to reduce spike-wave seizure counts. Respiration during high CO_2 causes hypercapnia, a condition that increases blood $PaCO_2$ and acidifies the blood (Eldridge et al., 1984). As with hypoxia, hypercapnia also triggers hyperventilation (Guyenet et al., 2019). We performed ECoG/plethysmography experiments in rats that cycled through trials of normoxia and hypercapnia (21% O_2; 5% CO_2; 74% N_2) and compared the mean number of seizures observed during the two conditions. Relative to normoxia, the number of spike-wave seizures was lower during 5% CO_2 ($p = 0.0028$, $n = 8$; Figure 4B1 and 4C); hypercapnia also induced a powerful respiratory response ($p = 3.78 \times 10^{-5}$, $n = 8$; Figure 4B2,3 and 4D). Blood gas measurements revealed that 5% hypercapnia increased $PaCO_2$ ($p = 0.022$, $n = 6$; Figure 4E2) and slightly acidified blood pH ($p = 0.00063$, $n = 6$; Figure 4E3). These results provide further support for the hypothesis that the neural circuits that produce spike-wave seizures are CO_2-sensitive, and thus pH-sensitive. Moreover, the results demonstrate that neither the mechanics of elevated ventilation, nor increased arousal, is sufficient to provoke spike-wave seizures.

Optogenetic stimulation of the retrotrapezoid nucleus provokes spike-wave seizures

In addition to inducing hyperventilation and hypocapnia, hypoxia also lowers PaO_2 (see Figure 3H1), an effect that stimulates the carotid body, the principal peripheral chemoreceptor that initiates hyperventilation during hypoxic conditions (Lindsey et al., 2018; López-Barneo et al., 2016; Semenza & Prabhakar, 2018). Carotid body activity recruits neurons of the nucleus tractus solitarius (NTS) that then excite neurons of the central respiratory pattern generator to drive a respiratory response (Guyenet, 2014; López-Barneo et al., 2016). To evaluate the capacity of hyperventilation to provoke seizures in the absence of hypoxia (and, therefore, in the absence of

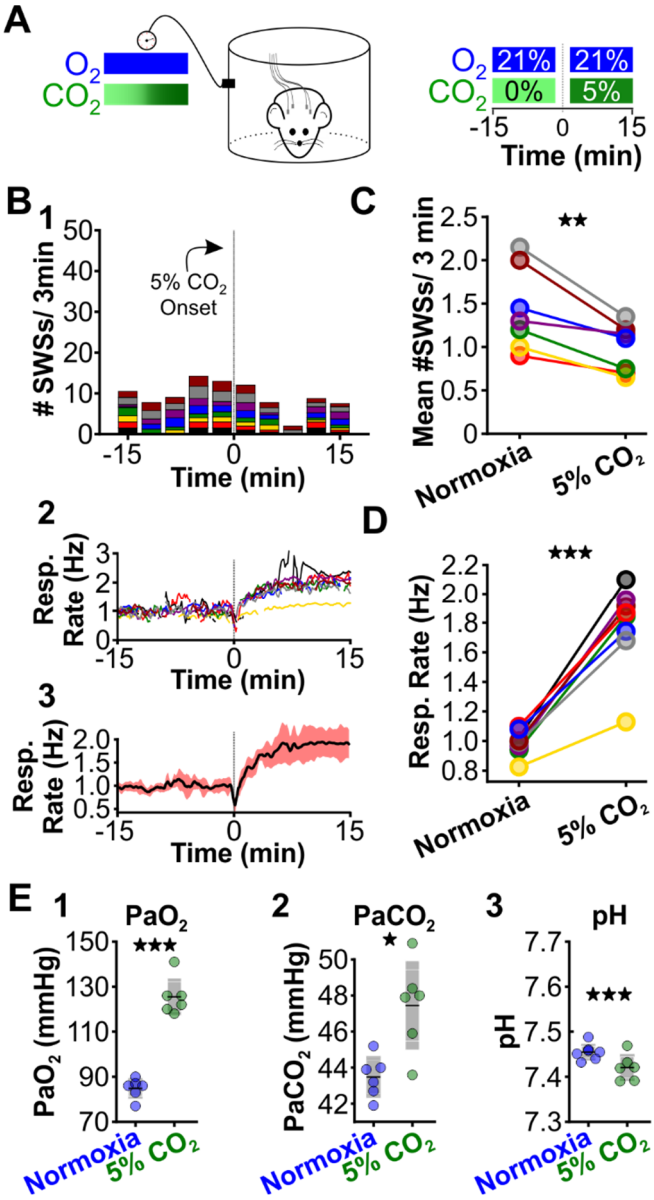

Figure 4. Supplemental CO_2 suppresses spontaneous spike-wave seizures.
(A) Experimental approach. Plethysmography chambers recorded ventilation and ECoG/EMG signals in WAG/Rij rats exposed to normoxia (i.e., 21% O_2) and hypercapnia (i.e., 21% O_2, 5% CO_2). **(B)** Spike-wave seizure (SWS) and respiratory quantification. (1) Stacked histogram illustrating spike-wave seizure count for each animal before and after the onset of hypercapnia. (2) Corresponding respiratory rate for each animal shown in panel B1. (3) Mean respiratory rate for all animals. **(C)** Mean spike-wave seizure count per bin and **(D)** respiratory rate before and after hypercapnia exchange. **(E)** Arterial measurements in the same rats show that hypercapnia produced a predictable increase in arterial (1) O_2 and (2) CO_2, as well as (3) respiratory acidosis. Increase arterial O_2 reflects robust ventilatory response during hypercapnia. See **Tables 1, 2 and 4** for detailed statistics. *p < 0.05, **p < 0.01, ***p < 0.001.

carotid body activation), we utilized an alternative approach to induce hyperventilation. Under physiological conditions, chemosensitive neurons of the retrotrapezoid nucleus (RTN), a brainstem respiratory center, are activated during an increase in $PaCO_2$ and a consequent drop in arterial pH (Guyenet et al., 2016, 2019; Guyenet & Bayliss, 2015) that then stimulate respiration. Optogenetic activation of RTN neurons in normoxia is sufficient to evoke a powerful hyperventilatory response that alkalizes the blood (Abbott et al., 2011; Souza et al., 2020). Importantly, PaO_2 remains stable (or is slightly elevated) during optogenetically-induced respiration. Therefore, hyperventilation evoked by optogenetic RTN activation during normoxia both (1) promotes respiratory alkalosis without hypoxia and (2) is a more clinically relevant approximation of voluntary hyperventilation than hypoxia-induced hyperventilation.

We selectively transduced RTN neurons of WAG/Rij rats with a lentiviral approach using the PRSX8 promoter to drive channelrhodopsin expression (Abbott et al., 2009; Hwang et al., 2001; Lonergan et al., 2005). Once channelrhodopsin was expressed, we challenged rats with two test trials: RTN photostimulation during normoxia and RTN photostimulation during hypercapnia (Figure 5A); in a subset of animals, we cycled rats between the two conditions. In both trials, the laser was pulsed at 20 Hz (10msec pulse) once every four seconds for two seconds. Laser stimulation during normoxia provoked spike-wave seizures ($p = 0.002$; $n = 10$; Figures 5B, 5C1 and 5D) and also increased ventilation ($p = 0.019$; $n = 10$; Figures 5C2,3 and 5E). In contrast, laser stimulation during hypercapnia in the same animals did not alter spike-wave seizure count ($p = 0.86$; $n = 6$; Figures 5F1 and 5G), despite the induction of a strong hyperventilatory response ($p = 0.031$; $n = 6$; Figures 5F2,3 and 5H). In sum, these results support the hypothesis that respiratory alkalosis is necessary to provoke seizures during hyperventilation and excludes carotid body activation as a contributing factor.

Hypoxia-induced hyperventilation activates neurons of the intralaminar thalamus

Thus far, our results demonstrated that respiratory alkalosis (i.e., hyperventilation that

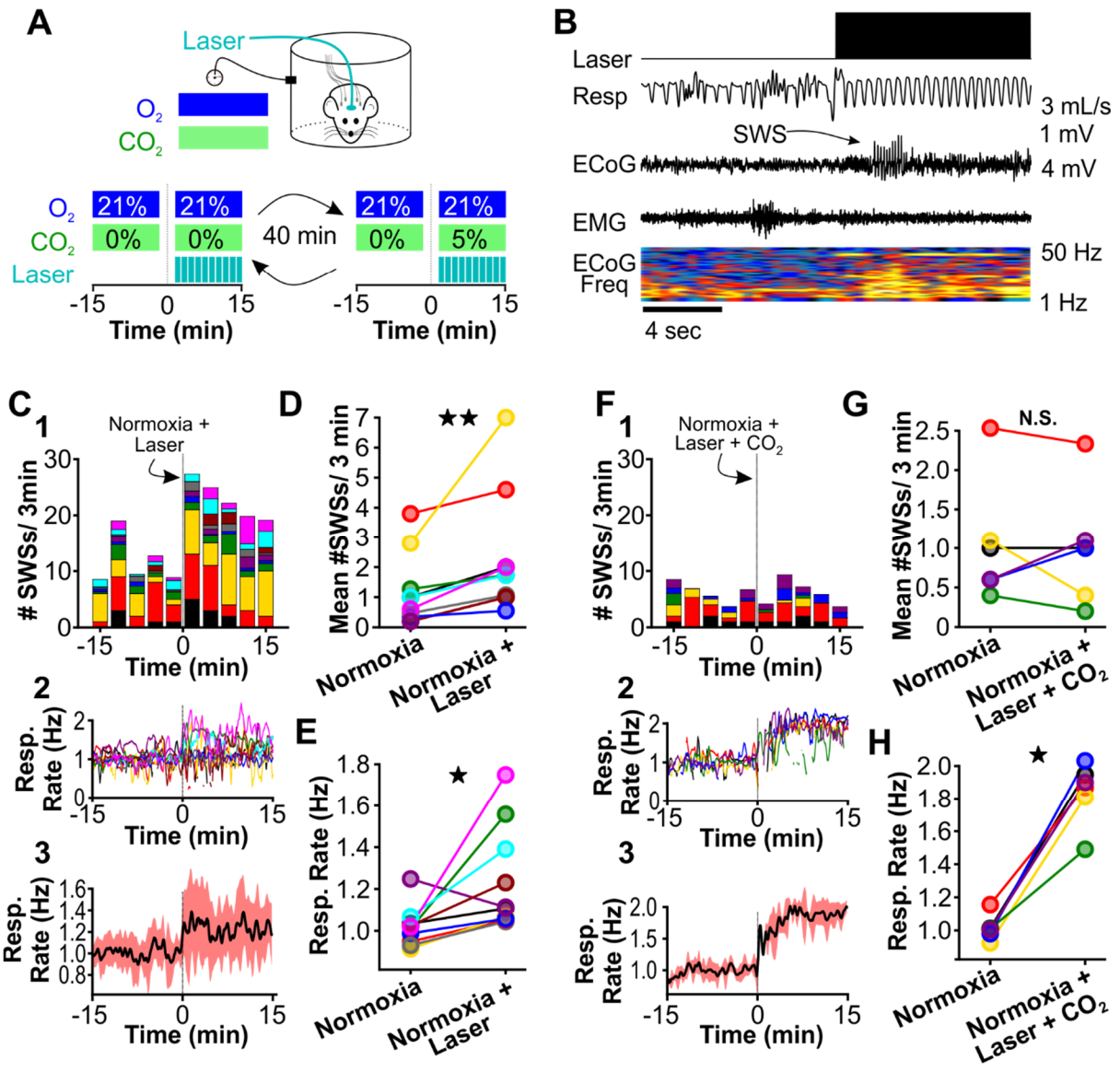

Figure 5. Normoxic hyperventilation provokes CO_2-sensitive spike-wave seizures.
(A) Experimental approach. Plethysmography chambers recorded ventilation and ECoG/EMG signals in WAG/Rij rats exposed to normoxia (i.e., 21% O_2) and normoxia + CO_2, (i.e., 10% O_2, 5% CO_2). Channelrhodopsin-mediated photostimulation of the retrotrapezoid nucleus (RTN) was used to increase ventilation. **(B)** Example of ventilatory response and spike-wave seizure during normoxic RTN photostimulation **(C-E)** RTN photostimulation during normoxia. **(C)** Spike-wave seizure (SWS) and respiration quantification. (1) Stacked histogram illustrating spike-wave seizure count for each animal before and after normoxia photostimulation onset. (2) Corresponding respiratory rate for each animal shown in panel C1. (3) Mean respiratory rate for all animals. **(D)** Mean spike-wave seizure count per bin and **(E)** respiration rate before and after normoxia photostimulation onset. **(F-H)** RTN photostimulation during hypercapnia (i.e., 21% O_2, 5% CO_2). **(F)** Spike-wave seizure and respiratory quantification. (1) Stacked histogram illustrating spike-wave seizure count for each animal before and after hypercapnic photostimulation onset. (2) Corresponding respiratory rate for each animal shown in panel F1. (3) Mean respiratory rate

for all animals. **(G)** Mean spike-wave seizure count per bin and **(H)** respiratory rate before and after hypercapnic photostimulation onset. See **Tables 1, 2 and 4** for detailed statistics. *p < 0.05, **p < 0.01, not significant (n.s.).

promotes a net decrease in $PaCO_2$) provokes spike-wave seizures in the WAG/Rij rat. Next, we sought to identify brain structures activated during respiratory alkalosis that may contribute to spike-wave seizure provocation. We used the neuronal activity marker cFos to identify such structures in WAG/Rij rats. To isolate activation specifically associated with respiratory alkalosis, we first administered ethosuximide (200mg/kg, i.p.) to suppress spike-wave seizures; respiration and ECoG/EMG signals confirmed ventilatory responses and spike-wave seizure suppression. Ethosuximide-injected rats were exposed to either hypoxia, normoxia or hypoxia/hypercapnia for 30 minutes and then transcardially perfused 90 minutes later. Brains were harvested and evaluated for cFos immunoreactivity. Surprisingly, in rats exposed to hypoxia we observed heightened immunoreactivity in the intralaminar nuclei, a group of higher-order thalamic nuclei that, unlike first-order thalamic nuclei, do not receive peripheral sensory information (Saalmann, 2014) (Figure 6A,B). Indeed, cFos immunoreactivity was largely absent from first-order thalamic nuclei and cortex, and was blunted in rats treated with normoxia and hypoxia/hypercapnia (Figure 6B). Importantly, the latter condition elevates respiration but normalizes arterial pH (see Figure 3G and 3H). Immunoreactivity quantification revealed that the number of cFos-positive cells within the intralaminar thalamic nuclei was highest following hypoxia [ANOVA: $F(2, 6) = 31.59$, $p = 0.00019$, Figure 6C].

As heightened cFos immunoreactivity was observed primarily following hypoxia that results in pronounced respiratory alkalosis, we next tested the hypothesis that neurons of the intralaminar nuclei are pH-sensitive. We stereotaxically delivered the pan-neuronal expressing GCaMP7s (pGP-AAV-syn-jGCaMP7s-WPRE) to the intralaminar nuclei and harvested acute brain sections three weeks later (Figure 6D). Recording fluorescence changes in brain sections revealed that extracellular alkalosis quickly and reversibly activated neurons of the intralaminar

nuclei (Figure 6D). Collectively, these results support the hypothesis that respiratory alkalosis activates pH-sensitive neurons of the intralaminar thalamic nuclei in the WAG/Rij rat.

Discussion

Hyperventilation-provoked seizures associated with absence epilepsy were first formally described in 1928 by William Lennox (Lennox, 1928) and despite the clinical ubiquity of utilizing hyperventilation to diagnose the common form of childhood epilepsy, no animal studies have attempted to resolve the physiological events that enable hyperventilation to reliably provoke spike-wave seizures. To resolve events and relevant brain structures recruited during this phenomenon, we first utilized the WAG/Rij rat to establish a rodent model that mimics hyperventilation-provoked spike-wave seizures in humans. With this model, we show that hyperventilation only provokes spike-wave seizures in seizure-prone, not generally seizure-free, rats. We then show that supplemental CO_2, by mitigating respiratory alkalosis, suppresses spike-wave seizures triggered by hyperventilation during either hypoxia or direct activation of brainstem respiratory centers. Moreover, supplemental CO_2, by producing respiratory acidosis, suppresses spontaneous spike-wave seizures (i.e., those occurring during normoxia) despite a compensatory increase in respiratory rate. These data demonstrate that spike-wave seizures are yoked to arterial CO_2/pH. Finally, we demonstrate that respiratory alkalosis activates neurons of the intralaminar thalamic nuclei, also in a CO_2-dependent manner; activation of these neurons is also pH-sensitive. With these observations, we propose a working model wherein respiratory alkalosis activates pH-sensitive neurons of the intralaminar nuclei that in turn engage seizure-generating neural circuits to produce spike-wave seizures (Figure 7).

Cortical EEG Patterns Evoked by Hyperventilation

Hyperventilation produces stereotypical EEG patterns in both healthy children and children with absence epilepsy (Barker et al., 2012). In healthy children, hyperventilation can

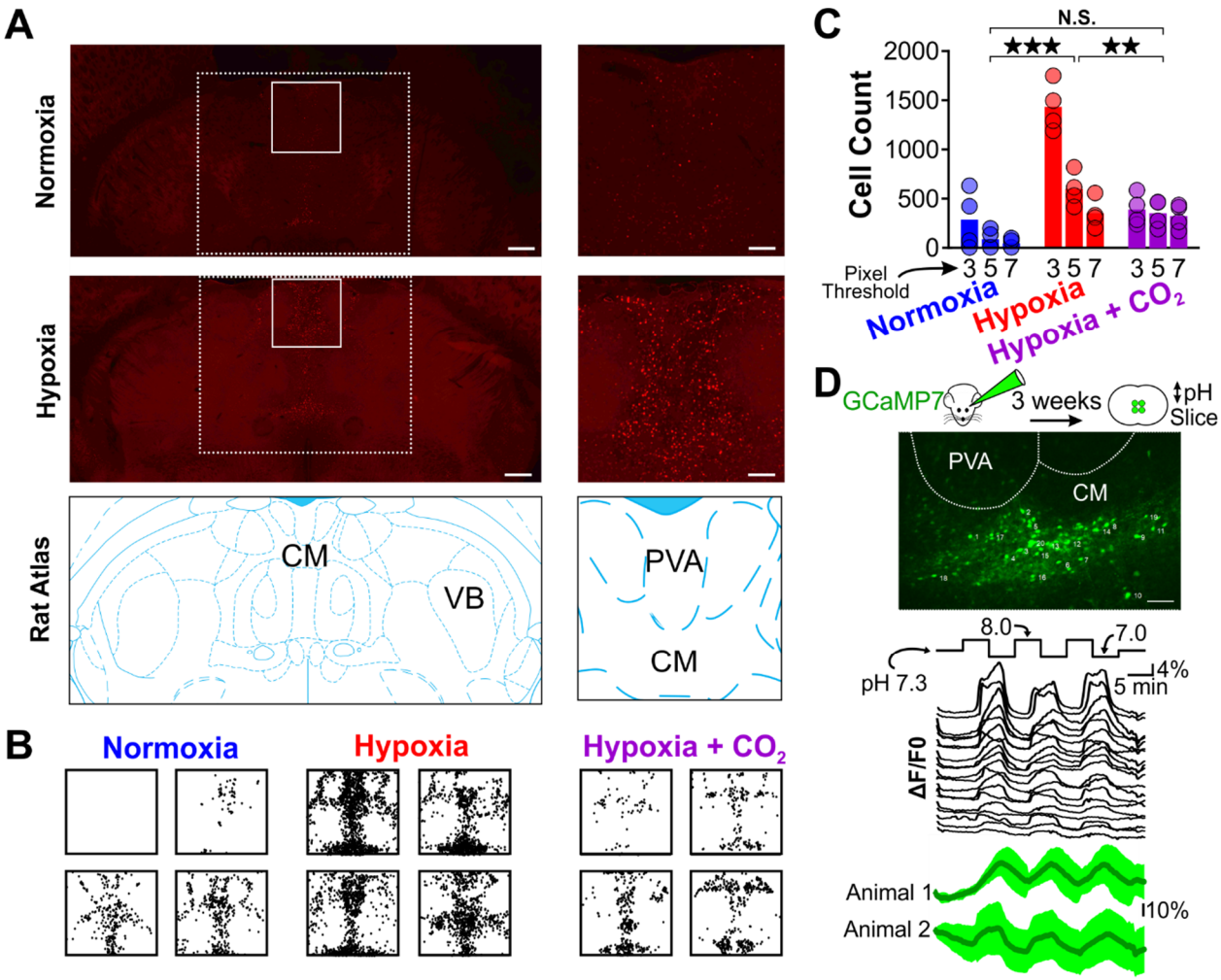

Figure 6. Hypoxia-induced hyperventilation activates intralaminar thalamic neurons. **(A)** cFos immunohistochemistry in horizontal sections of the WAG/Rij rat. Dashed lines highlight the medial region of the thalamus containing the intralaminar nuclei. Solid lines demarcate regions containing elevated cFos expression and are expanded on right. Top images are collected from a rat exposed to 30 minutes of normoxia. Middle images are collected from a rat exposed to 30 minutes of hypoxia. Bottom images are taken from Paxinos and Watson (Paxinos & Watson, 2007) and show the structural landmarks in the top and middle images. The central median nucleus (CM, intralaminar thalamus) and ventrobasal complex (VB, first-order thalamus) are labeled. **(B)** cFos density plots show immunoreactivity in each of four rats exposed to either normoxia, hypoxia or hypoxia + CO_2. Each black dot represents a cFos-positive cell, as identified with ImageJ (see Methods). Plots are aligned to expanded views in panel A. **(C)** Quantification of cFos labeled cells at different ImageJ thresholding values. **(D)** GCaMP7 was stereotaxically delivered to the intralaminar nuclei. Later, fluorescence changes were measured during extracellular alkaline challenges in acute slices containing the intralaminar nuclei. Individual ROIs show fluorescence changes during alkalosis (black traces). Mean responses from two animals are shown in green. $^{**}p < 0.01$, $^{***}p < 0.001$. See **Table 5** for detailed statistics. Scale bars are 500 μm (*left*) and 100 μm *(right)*.

464 evoke an EEG pattern known as *Hyperventilation-Induced, High-Amplitude Rhythmic Slowing*
465 (HIHARS) that is often associated with altered awareness (Barker et al., 2012; Lum et al., 2002).
466 Electrographically, HIHARS is distinct from spike-wave seizures insofar the EEG lacks epilepsy-
467 associated spikes and resembles slow-wave sleep. Nonetheless, similarities between HIHARS
468 and absence seizures exist. Both events are associated with children of the same age (Mattozzi
469 et al., 2021). Behaviorally, eye opening/staring and fluttering, as well as oral automatisms, are
470 observed during both events, albeit with different frequencies (Lum et al., 2002). Finally, the mean
471 latencies from the onset of hyperventilation to the onset of electrographic HIHARS in healthy
472 children, or spike-wave seizures in absence patients, are also similar (Lum et al., 2002; Mattozzi
473 et al., 2021).

474 Recent work suggests that spike-wave seizures may limit or preclude the generation of
475 HIHARs in children with absence epilepsy, thereby supporting the hypothesis that HIHARS and
476 spike-wave seizures borrow from similar neural circuit mechanisms (Mattozzi et al., 2021). In this
477 model, hyperventilation engages brain structures that initiate and/or support widespread,
478 synchronous cortical activity. However, the trajectory of this engagement ultimately bifurcates
479 such that either HIHARS or a spike-wave seizure is produced, but not both. When viewed
480 alongside work performed in the 1960s by Ira Sherwin (Sherwin, 1965, 1967), our results support
481 this model. Sherwin demonstrated that hyperventilation evokes HIHARS in cats (Sherwin, 1965),
482 and that the stereotyped EEG pattern requires an intact central lateral nucleus of the thalamus
483 (Sherwin, 1967). Together with the central medial (CM) and paracentral thalamic nuclei, the
484 central lateral nucleus belongs to the anterior group of the intralaminar nuclei (Saalmann, 2014),
485 the location of cFos immunoreactivity associated with respiratory alkalosis and pH-sensitivity
486 (Figure 6). Indeed, at the time Sherwin postulated that the intralaminar nuclei of the thalamus are
487 both chemoreceptive and capable of engaging widespread cortical activity (Sherwin, 1967). We
488 now postulate that these nuclei are also instrumental for provoking spike-wave seizures during
489

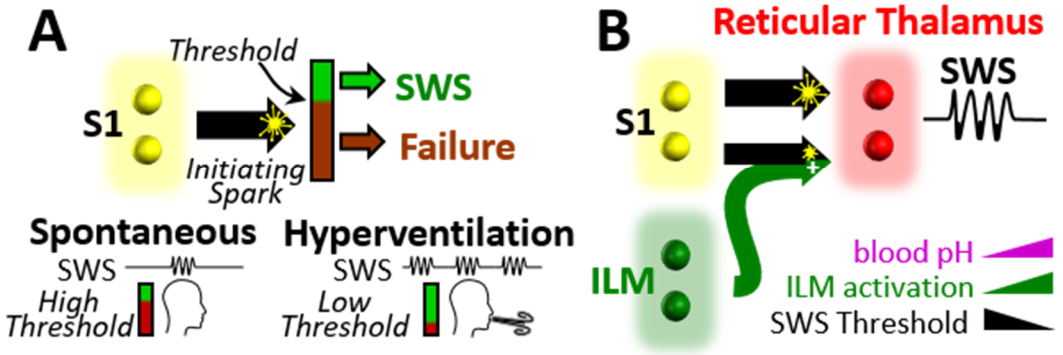

Figure 7. Working model. **A.** Spike-wave seizures only occur if initiating activity from S1 somatosensory cortex successfully overcomes a threshold, consistent with the cortical focus theory (H. K. M. Meeren et al., 2002). Hyperventilation-associated alkalosis reduces spike-wave seizure (SWS) threshold. **B.** S1 initiating activity is proposed to overcome a seizure node formed by circuits in reticular thalamus to generate an spike-wave seizure (Paz & Huguenard, 2015). We propose that hyperventilation-evoked respiratory alkalosis activates the intralaminar nuclei (ILM) to reduce the threshold for S1 activity required to evoke a spike-wave seizure.

hyperventilation. If true, then resolving how and where the mechanisms that produce HIHARS diverge from those that produce spike-wave seizures becomes a central goal.

Thalamocortical circuit involvement in spike-wave seizures

Decades of work have culminated in a canonical model wherein interconnected circuits between the cortex and thalamus support the initiation and maintenance of generalized spike-wave seizures (Avoli, 2012; Beenhakker & Huguenard, 2009; Huguenard & McCormick, 2007; McCafferty et al., 2018; McCormick & Contreras, 2001; Meeren et al., 2002). By recording from multiple sites in the WAG/Rij rat, Meeren et al. (Meeren et al., 2002) concluded that the peri-oral region of somatosensory cortex provides the bout of hypersynchronous activity that initiates a spike-wave seizure. This activity then rapidly recruits additional somatosensory cortices and the lateral dorsal thalamus, a higher-order thalamic nucleus involved in spatial learning and memory (Bezdudnaya & Keller, 2008). Finally, first-order thalamic nuclei that encode somatosensory information (i.e., the ventrobasal complex) are recruited. This stereotyped succession of events occurs within the first 500 milliseconds of the spike-wave seizure, after which the temporal relationships among cortical and thalamic structures are more unpredictable (Meeren et al., 2002). Additional studies support the hypothesis that cortical hyperactivity initiates spike-wave seizures (Pinault, 2003; Pinault et al., 1998) and have motivated what is generally referred to as the *cortical focus theory* for spike-wave seizure initiation (Meeren et al., 2005).

While resolving how seizures initiate and propagate through brain structures is of critical importance, this understanding does not necessarily address the mechanisms that drive the highly rhythmic and hypersynchronous activity associated with ongoing spike-wave seizures. Extensive work on acute brain slice preparations clearly demonstrates that circuits between first-order thalamic nuclei and the reticular thalamic nucleus are sufficient to sustain rhythmic network activities, including those comparable to absence seizures (Bal et al., 1995; Bal & McCormick, 1993; McCormick & Contreras, 2001; von Krosigk et al., 1993). In this model, feedforward

546 inhibition provided by reticular neurons evokes robust, hypersynchronous post-inhibitory rebound
547 bursts among thalamocortical neurons that then relay activity back to reticular thalamus and to
548 cortex. Reticular neuron-mediated feedforward inhibition of thalamocortical neurons, coupled with
549 reciprocal excitation from thalamocortical neurons to reticular neurons, forms the basis of a
550 rhythmogenic circuit that is proposed to maintain spike-wave seizures. While this model very
551 likely accounts for rhythmicity in the acute brain slice preparation, it is becoming less clear how
552 first-order thalamocortical neurons actively contribute to the maintenance of spike-wave seizures
553 recorded *in vivo* (Huguenard, 2019; McCafferty et al., 2018). Moreover, most current models of
554 spike-wave initiation and maintenance neglect the potential contribution of the intralaminar nuclei
555 to seizure initiation and maintenance despite several observations to the contrary.

556 In an effort to resolve structures capable of evoking spike-wave seizures, Jasper and
557 colleagues electrically stimulated several thalamic nuclei in cats while recording EEG. By doing
558 so in both lightly anesthetized (Jasper & Droogleever-Fortuyn, 1947) and unanesthetized (Hunter
559 & Jasper, 1949) animals, the authors concluded that stimulation of the anterior intralaminar nuclei
560 (i.e., central lateral, central medial and paracentral nuclei) was sufficient to evoke spike-wave
561 seizures that outlasted the stimulus; stimulation also produced behavioral repertoires associated
562 with absence seizures. However, stimulation of first-order thalamic nuclei did not evoke spike-
563 wave seizures, nor did it evoke seizure-like behaviors. Consistent with these observations, lesions
564 to the intralaminar nuclei abolish pharmacologically-induced spike-wave seizures in Sprague-
565 Dawley rats (Banerjee & Snead, 1994); seizures persist following lesions to first-order nuclei.
566 More recently, an EEG-fMRI study in human patients also implicates the intralaminar nuclei in the
567 initiation of spontaneous spike-wave seizures (Tyvaert et al., 2009). Regrettably, Meeren et al.
568 (Meeren et al., 2002) did not include intralaminar thalamic recordings during their study of spike-
569 wave seizure propagation in the WAG/Rij rat. Nonetheless, proposing the hypothesis that the
570 intralaminar nuclei, not cortical structures, initiate spike-wave seizures, including those occurring
571 spontaneously (i.e., not during hyperventilation), seems premature. Indeed, the possibility that

activation of cortically projecting intralaminar neurons during hyperventilation recruits cortical structures to, in turn, initiate spike-wave seizures is equally plausible (see Figure 7).

Thalamic pH sensitivity

First-order thalamic neurons express several pH-sensitive ion channels and receptors. TASK-1 and TASK-3, two TWIK-related acid-sensitive potassium channels, with the hyperpolarization-activated cyclic nucleotide–gated (HCN) ion channel, collectively play a critical role in stabilizing the resting membrane potential of first-order thalamic neurons (Meuth et al., 2003, 2006). When activated, TASK channels hyperpolarize the membrane potential of thalamocortical neurons. In contrast, HCN channels depolarize thalamocortical neuron membrane potential. As extracellular acidification inhibits the activity of both channels, the opposing actions of TASK and HCN channels are simultaneously downregulated to yield no net effect on thalamocortical neuron membrane potential (Meuth et al., 2006), thereby stabilizing the membrane potential during acidic conditions. While not yet directly tested, the opposing actions of TASK and HCN channels also presumably stabilize thalamocortical membrane potential during alkaline conditions. Thus, while first-order thalamocortical neurons express pH-sensitive ion channels, these neurons are presumed to maintain stable membrane potentials during extracellular pH fluctuations. If true, then first-order thalamic nuclei are unlikely to support an active role in initiating hyperventilation-provoked spike-wave seizures. The extent to which higher-order thalamic nuclei express TASK and HCH channels remains unknown.

Importantly, intralaminar neurons recruited during hyperventilation-mediated alkalosis may not reflect intrinsic pH sensitivity. Instead, activation of intralaminar neurons during alkalosis may result from increased excitatory synaptic input. Intralaminar neurons receive significant, monosynaptic excitation from the midbrain reticular formation (Ropert & Steriade, 1981; Steriade & Glenn, 1982); first-order thalamic nuclei only do so negligibly (Edwards & de Olmos, 1976). Several reticular nuclei are critically important for respiration (Guyenet & Bayliss, 2015; Smith et

al., 2013) and therefore provide clear rationale for testing the hypothesis that reticular-mediated excitation of the intralaminar nuclei drive hyperventilation-associated cFos expression (i.e., Figure 6). Notably, cFos expression was only observed during respiratory alkalosis (i.e., hypoxia) and not during hyperventilation associated with a normalized arterial pH (i.e., hypoxia-hypercapnia; c.f. Figures 3H and 6B). Thus, if reticular-mediated excitation of intralaminar neurons plays a role in hyperventilation-provoked spike-wave seizures, then it does so only during conditions of respiratory alkalosis. Finally, the possibility that the synaptic terminals of intralaminar-projecting afferents are pH-sensitive also warrants examination. Notably, solute carrier family transporters (SLC) shuttle H^+ and HCO_3^+ across neuronal membranes and are proposed to regulate seizures, including spike-wave seizures (Cox et al., 1997; Sander et al., 2002; Sinning & Hübner, 2013). Alkaline conditions enhance excitatory synaptic transmission, an effect attributed to Slc4a8, a Na^+-Driven Cl^-/Bicarbonate Exchanger (Sinning et al., 2011; Sinning & Hübner, 2013), that is expressed in the presynaptic terminals of excitatory neurons, including those in the thalamus (Lein et al., 2007). Thus, the potentiation of intralaminar neuron excitation remains a plausible candidate mechanism to explain the observed cFos expression during respiratory alkalosis.

Conclusion

In aggregate, our data support the hypothesis that spike-wave seizures are yoked to arterial pH. The observation that respiratory alkalosis activates intralaminar thalamic neurons, and that such neurons are activated by alkaline conditions, reignites a 70-year-old hypothesis wherein intralaminar neurons actively participate in the initiation and maintenance of spike-wave seizures.

Material and Methods

Study Design

The goal of this study was to parameterize the effect of blood gases on spike-wave seizures. To do so, we adapted a clinically observed human phenomenon in absence epilepsy patients to a rodent model of spike-wave seizures. We demonstrate that spike-wave seizure occurrence correlates with rising or falling values of $PaCO_2$ and pH. Significantly, we show that neurons of the midline thalamus become activated after brief exposure to low $PaCO_2$ conditions. We propose that activity among pH-sensitive neurons in the thalamus, responsive to hyperventilation-induced hypocapnia, trigger spike-wave seizures. All physiology and ECoG/EMG recordings were performed in freely behaving WAG/Rij or Wistar rats. To reduce the number of animals, rats were exposed to multiple conditions. Experimenters were blinded to the condition for all respiration and ECoG/EMG data analysis. Group and sample size were indicated in the results section.

Animals

All procedures conformed to the National Institutes of Health *Guide for Care and Use of Laboratory Animals* and were approved by the University of Virginia Animal Care and Use Committee (Charlottesville, VA, USA). Unless otherwise stated, animals were housed at 23-25°C under an artificial 12 h light-dark cycle with food and water *ad libitum*. A colony of Wistar Albino Glaxo/from Rijswik (WAG/Rij rats) were kindly provided by Dr. Edward Bertram, University of Virginia) and maintained in the animal facilities at The University of Virginia Medical Center. Male Wistar IGS Rats were purchased from Charles River (Strain Code: #003). Plethysmography, EEG, blood gas measurements and c-Fos immunohistochemistry experiments were performed in 100+-day old WAG/Rij and Wistar rats as these ages correspond to when spike-wave seizures become robust in the WAG/Rij rat. Male and female rats were used in all experiments – no noticeable differences were observed. Of note, only male rats were used in optogenetic manipulations, as female rats were less likely to recover from surgery.

649 Animal Preparation

650 All surgical procedures were conducted under aseptic conditions. Body temperature was
651 maintained at 37°C. Animals were anesthetized with 1-3% isoflurane or a mixture of ketamine (75
652 mg/kg), xylazine (5 mg/kg) and acepromazine (1 mg/kg) administered intra-muscularly. Depth of
653 anesthesia was monitored by lack of reflex response to a firm toe and tail pinch. Additional
654 anesthetic was administered during surgery (25% of original dose) if warranted. All surgeries,
655 except the arterial catheter implantation, were performed on a stereotaxic frame (David Kopf
656 Instruments, Tujunga, CA, USA). Post-operative antibiotic (ampicillin, 125 mg/kg) and analgesia
657 (ketoprofen, 3-5 mg/kg, subcutaneously) were administered and as needed for 3 days. Animals
658 recovered for 1-4 weeks before experimentation.

659

660 Electrocorticogram (ECoG) and electromyography (EMG) electrode implantation

661 Commercially available rat recording devices were purchased from Plastics One
662 (Roanoke, VA, USA). Recording electrodes were fabricated by soldering insulated stainless-steel
663 wire (A-M system, Sequim, WA, USA) to stainless-steel screws (Plastics One) and gold pins
664 (Plastics One). On the day of surgery, a small longitudinal incision was made along the scalp.
665 Small burr holes were drilled in the skill and ECoG recording electrodes were implanted bilaterally
666 in the cortex. Reference electrodes were placed in the cerebellum. A twisted-looped stainless-
667 steel wire was sutured to the superficial neck muscles for EMG recordings. The recording device
668 was secured to the skull with dental cement and incisions were closed with absorbable sutures
669 and/or steel clips.

670

671 PRSX-8 lentivirus preparation

672 The lentivirus, *PRSX8*-hCHR2(H134R)-mCherry, was designed and prepared as
673 described previously (Abbott et al., 2009). Lentivirus vectors were produced by the Salk Institute
674 Viral Vector Core. The titer for the *PRSX8*-hCHR2(H134R)-mCherry lentivirus was diluted to a

675 working concentration of 1.5 x 10^{10} TU/mL. The same batch of virus was used for all experiments
676 included in this study.
677
678 Virus injection and fiber optic ferrule implantation
679 Borosilicate glass pipettes were pulled to an external tip diameter of 25 μm and backfilled
680 with the lentivirus, *PRSX8*-hCHR2(H134R)-mCherry. Unilateral virus injections in the RTN were
681 made under electrophysiological guidance of the antidromic potential of the facial nucleus (see
682 Abbott et al., 2009; Souza et al., 2018). A total of 400 nL was delivered at three rostro caudal
683 sites separated by 200 or 300 μm in the RTN. Illumination of the RTN was performed by placing
684 a 200-μm-diameter fiber optic (Thor Labs, #BFL37-200; Newton, NJ, USA) and ferrule (Thor Labs,
685 #CFX128-10) vertically through the cerebellum between 300-1000 μm dorsal to RTN ChR2-
686 expressing neurons. These animals were also implanted with ECoG/EMG recording electrodes,
687 as detailed above. All hardware was secured to the skill with dental cement. Animals recovered
688 for 4 weeks, as this provided sufficient time for lentivirus expression in the RTN. Virus injection
689 location was verified post-hoc. Only animals that responded to optical stimulation, demonstrated
690 by an increase in respiratory frequency, were included in the results.
691
692 Physiology experiments in freely behaving rats
693 All experiments were performed during the dark cycle (hours 0-4) at ambient room
694 temperature of 27°C-28°C. Rats were habituated to experimental conditions for a minimum of 4
695 hours, 1-2 d before experiment start. On the day of recordings, rats were briefly anesthetized with
696 3% isoflurane for < 5min to connect the ECoG/EMG recording head stage to a recording cable
697 and, when necessary, to connect the fiber optic ferrule to a fiber optic cord (multimode 200μm
698 core, 0.39 nA) attached to a 473 nm blue laser (CrystaLaser model BC-273-060-M, Reno, NV,
699 USA). Laser power was set to 14mW measured at the junction between the connecting fiber and

the rat. Rats were then placed immediately into a whole-body plethysmography chamber (5L, EMKA Technologies, Falls Church, VA, USA). Recordings began after 1 h of habituation. The plethysmography chamber was continuously perfused with room air or protocols cycling through specific gas mixtures of O_2, N_2 and CO_2 (total flow: 1.5 L/min). Mass flow controllers, operated by a custom-written Python script, regulated gas exchange. Respiratory flow was recorded with a differential pressure transducer. The respiratory signal was filtered and amplified at 0.1-100 Hz, X 500 (EMKA Technologies). Respiratory signals were digitized at 200 Hz (CED Instruments, Power1401, Cambridge, England). ECoG and EMG signals were amplified (X1000, Harvard Apparatus, Holliston, MA, USA; Model 1700 Differential Amplifier, A-M Systems), bandpass filtered (ECoG: 0.1-100 Hz; EMG: 100-300 Hz) and digitized at 200 Hz. Respiratory flow, ECoG/EMG recordings, O_2 flow and the laser pulse protocol were captured using Spike2, 7.03 software (CED Instruments). Spike-wave seizure occurrence before and during specific conditions is shown as a peri-stimulus time histogram aligned at time = 0 at gas exchange onset or laser-on for optogenetic stimulations. Spike-wave seizure counts were quantified in 3 bins beginning +/- 15 minutes of gas exchange or laser onset. Total spike-wave seizure counts were obtained by summing the number of spike-wave seizures between -15 and 0 minutes (control) and 0 and +15 minutes (manipulation). Respiratory frequency (f_R, in breaths/minute) was derived from the respiration trace. The respiration trace was divided into individual windows, each 10 seconds in duration, and a fast Fourier transform (FFT) was computed on each discrete window. The respiratory rate for each window was defined by the FFT frequency with the maximal power density. Once derived for each window, we then applied a 30-second moving average to smooth the trace. RTN neurons were optically stimulated with 10 ms pulses delivered at 20 Hz for 2 seconds, followed by 2 seconds rest. This stimulation protocol was repeated for 20 minutes.

Femoral artery catheterization, blood gases and pH measurements.

Arterial blood samples for blood gas measurements through an arterial catheter during physiological experiments. One day prior to the experiments, rats anesthetized with isoflurane (2% in pure O_2) and a polyethylene catheter (P-10 to P-50, Clay Adams, Parsippany, NJ, USA) was introduced into the femoral artery by a small skin incision towards the abdominal aorta. The catheter was then tunneled under the skin and exteriorized between the scapulae with two inches of exposed tubing anchored with a suture. On the day of the experiment, animals were briefly anesthetized with 1-2% isoflurane to attach tubing for blood collection before placement into the plethysmography recording chamber. Arterial blood gases and pH were measured using a hand-held iStat configured with CG8+ cartridges (Abbott Instruments, Lake Bluff, USA).

cFos Histology

After exposing WAG/Rij rats to 30 minutes of hypoxia (10% O_2; 90% N_2) or hypoxia/hypercapnia (10% O_2; 5% CO_2; 75% N_2) rats were deeply anesthetized and perfused transcardially with 4% paraformaldehyde (pH 7.4). Brains were removed and post-fixed for 12-16 h at 4 °C. 40µm horizontal sections of the thalamus (D/V depth -5.3 mm to 6.0 mm) were obtained using a Leica VT 1000S microtome (Leica Biostystems, Buffalo Grove, IL, USA) and collected in 0.1 M phosphate buffer (PB) with 0.1% sodium azide (Millipore-Sigma, St. Louis, MO, USA). Sections were then transferred to a 0.1M PB solution containing 20% sucrose for 1hr, snap-frozen and transferred to 0.1% sodium borohydride for 15 minutes. Slices were washed 2x in phosphate buffered saline (PBS). All blocking and antibody solutions were prepared in an incubation buffer of 0.1% sodium azide, 0.5% Triton X-100 and 2% normal goat serum. Sections were blocked for 4hrs at room temperature or overnight at 4°C in incubation buffer. Sections were washed 3x with PBS between primary and secondary antibody solutions. Primary antibody solutions containing rabbit anti-cFos (1:2000; Cell Signaling Technology Cat# 2250, RRID: AB_2247211, Danvers, MA, USA) and biotin (1:200, Jackson ImmunoResearch, West Grove, PA; RRID: AB_2340595) were prepared in incubation buffer and incubated overnight at 4°C. Sections were then incubated

751 overnight in secondary antibody solutions containing donkey strepavidin-Cy3 (1:1000, Jackson
752 ImmunoResearch; RRID: AB_2337244). Immunohistochemical controls were run in parallel on
753 spare sections by omitting the primary antisera and/or the secondary antisera. Sections from each
754 well were mounted and air-dried overnight. Slides were cover-slipped with VectaShield
755 (VectorLabs, Burlingame, CA) with the addition of a DAPI counterstain. All images were captured
756 with a Z1 Axioimager (Zeiss Microscopy, Thornwood, NY, USA) with computer-driven stage
757 (Neurolucida, software version 10; MicroBrightfield, Inc., Colchester, VT, USA). Immunological
758 sections were examined with a 10x objective under epifluorescence (Cy3). All sections were
759 captured with similar exposure settings. Images were stored in TIFF format and imported into
760 ImageJ (NIH). Images were adjusted for brightness and contrast to reflect the true rendering as
761 much as possible.
762
763 Calcium Imaging
764 pGP-AAV-syn-jGCaMP7s-WPRE (Addgene #104487-AAV9) was stereotaxically delivered to the
765 central median thalamic nucleus in P20-30 rats with sterile microliter calibrated glass pipettes. A
766 picospritzer (Picospritzer III, Parker Hannifin) was used to deliver 100-200 nl of virus. Three weeks
767 later, animals were sacrificed and their brains harvested for acute brain slice preparation. Animals
768 were deeply anesthetized with pentobarbital and then transcardially perfused with an ice-cold
769 protective recovery solution containing the following (in mm): 92 NMDG, 26 NaHCO3, 25 glucose,
770 20 HEPES, 10 MgSO4, 5 Na-ascorbate, 3 Na-pyruvate, 2.5 KCl, 2 thiourea, 1.25 NaH2PO4, 0.5
771 CaCl2, titrated to a pH of 7.3–7.4 with HCl (Ting et al., 2014). Horizontal slices (250 µm) containing
772 the intralaminar thalamic nuclei were cut in ice-cold protective recovery solution using a vibratome
773 (VT1200, Leica Biosystems) and then transferred to protective recovery solution maintained at
774 32–34°C for 12 min. Brain slices were kept in room temperature artificial cerebrospinal fluid
775 (ACSF) containing (in mm): 3 KCl, 140 NaCl, 10 HEPES, 10 Glucose, 2 MgCl2, 2 CaCl2. The
776 solution was bubbled with 100% O2 and the pH was set by adding varied amounts KOH.

Fluorescence signals were measured with a spinning disk confocal microscope outfitted with an sCMOS camera (ORCA-Flash4.0, Hamamatsu).

Data analysis and statistics

Statistical analyses were performed in GraphPad Prism v7 (San Diego, CA, USA). All data were tested for normality before additional statistical testing. Statistical details, including sample size, are found in the results section and corresponding supplemental tables. Either parametric or non-parametric statistical analyses were performed. A significance level was set at 0.05. Data are expressed as mean ± SEM.

References

Abbott, S. B. G., Stornetta, R. L., Coates, M. B., & Guyenet, P. G. (2011). Phox2b-Expressing Neurons of the Parafacial Region Regulate Breathing Rate, Inspiration, and Expiration in Conscious Rats. *Journal of Neuroscience*, *31*(45), 16410–16422. https://doi.org/10.1523/JNEUROSCI.3280-11.2011

Abbott, S. B. G., Stornetta, R. L., Fortuna, M. G., Depuy, S. D., West, G. H., Harris, T. E., & Guyenet, P. G. (2009). Photostimulation of Retrotrapezoid Nucleus Phox2b-Expressing Neurons In Vivo Produces Long-Lasting Activation of Breathing in Rats. *Journal of Neuroscience*, *29*(18), 5806–5819. https://doi.org/10.1523/JNEUROSCI.1106-09.2009

Adams, D. J., & Lueders, H. (1981). Hyperventilation and 6-hour EEG recording in evaluation of absence seizures. *Neurology*, *31*(9), 1175–1177. https://doi.org/10.1212/wnl.31.9.1175

Amengual-Gual, M., Sánchez Fernández, I., & Loddenkemper, T. (2019). Patterns of epileptic seizure occurrence. *Brain Research*, *1703*, 3–12. https://doi.org/10.1016/j.brainres.2018.02.032

Avoli, M. (2012). A brief history on the oscillating roles of thalamus and cortex in absence seizures. *Epilepsia*, *53*(5), 779–789. https://doi.org/10.1111/j.1528-1167.2012.03421.x

Bal, T., & McCormick, D. A. (1993). Mechanisms of oscillatory activity in guinea-pig nucleus reticularis thalami in vitro: A mammalian pacemaker. *The Journal of Physiology*, *468*(1), 669–691. https://doi.org/10.1113/jphysiol.1993.sp019794

Bal, T., von Krosigk, M., & McCormick, D. A. (1995). Role of the ferret perigeniculate nucleus in the generation of synchronized oscillations in vitro. *The Journal of Physiology*, *483*(3), 665–685. https://doi.org/10.1113/jphysiol.1995.sp020613

Banerjee, P. K., & Snead, O. C. (1994). Thalamic mediodorsal and intralaminar nuclear lesions disrupt the generation of experimentally induced generalized absence-like seizures in rats. *Epilepsy Research*, *17*(3), 193–205. https://doi.org/10.1016/0920-1211(94)90050-7

Barker, A., Ng, J., Rittey, C. D. C., Kandler, R. H., & Mordekar, S. R. (2012). Outcome of children with hyperventilation-induced high-amplitude rhythmic slow activity with altered awareness. *Developmental Medicine and Child Neurology*, *54*(11), 1001–1005. https://doi.org/10.1111/j.1469-8749.2012.04337.x

Bartolini, E., & Sander, J. W. (2019). Dealing with the storm: An overview of seizure precipitants and spontaneous seizure worsening in drug-resistant epilepsy. *Epilepsy & Behavior*, *97*, 212–218. https://doi.org/10.1016/j.yebeh.2019.05.036

Basting, T. M., Burke, P. G. R., Kanbar, R., Viar, K. E., Stornetta, D. S., Stornetta, R. L., & Guyenet, P. G. (2015). Hypoxia Silences Retrotrapezoid Nucleus Respiratory Chemoreceptors via Alkalosis. *The Journal of Neuroscience*, *35*(2), 527–543. https://doi.org/10.1523/jneurosci.2923-14.2015

Baud, M. O., Kleen, J. K., Mirro, E. A., Andrechak, J. C., King-Stephens, D., Chang, E. F., & Rao, V. R. (2018). Multi-day rhythms modulate seizure risk in epilepsy. *Nature Communications*, *9*(1), 1–10. https://doi.org/10.1038/s41467-017-02577-y

Bazil, C. W. (2019). Seizure modulation by sleep and sleep state. *Brain Research*, *1703*, 13–17. https://doi.org/10.1016/j.brainres.2018.05.003

Beenhakker, M. P., & Huguenard, J. R. (2009). Neurons that Fire Together Also Conspire Together: Is Normal Sleep Circuitry Hijacked to Generate Epilepsy? *Neuron*, *62*(5), 612–632. http://dx.doi.org/10.1016/j.neuron.2009.05.015

Bezdudnaya, T., & Keller, A. (2008). Laterodorsal Nucleus of the Thalamus: A Processor of Somatosensory Inputs. *The Journal of Comparative Neurology*, *507*(6), 1979–1989. https://doi.org/10.1002/cne.21664

848 Chen, T. T., Klassen, T. L., Goldman, A. M., Marini, C., Guerrini, R., & Noebels, J. L. (2013). Novel brain
849 expression of ClC-1 chloride channels and enrichment of CLCN1 variants in epilepsy. *Neurology*,
850 *80*(12), 1078–1085. https://doi.org/10.1212/WNL.0b013e31828868e7
851 Coenen, A. M. (2003). Genetic animal models for absence epilepsy: A review of the WAG/Rij strain of
852 rats. *Behavior Genetics*, *33*(6), 635–655.
853 Coenen, A. M., Drinkenburg, W. H., Inoue, M., & van Luijtelaar, E. L. (1992). Genetic models of absence
854 epilepsy, with emphasis on the WAG/Rij strain of rats. *Epilepsy Res.*, *12*, 75–86.
855 Cox, G. A., Lutz, C. M., Yang, C.-L., Biemesderfer, D., Bronson, R. T., Fu, A., Aronson, P. S., Noebels, J. L., &
856 Frankel, W. N. (1997). Sodium/Hydrogen Exchanger Gene Defect in Slow-Wave Epilepsy Mutant
857 Mice. *Cell*, *91*(1), 139–148. https://doi.org/10.1016/S0092-8674(01)80016-7
858 Crunelli, V., & Leresche, N. (2002). Childhood absence epilepsy: Genes, channels, neurons and networks.
859 *Nat Rev Neurosci*, *3*(5), 371–382.
860 Debski, K. J., Ceglia, N., Ghestem, A., Ivanov, A. I., Brancati, G. E., Bröer, S., Bot, A. M., Müller, J. A.,
861 Schoch, S., Becker, A., Löscher, W., Guye, M., Sassone-Corsi, P., Lukasiuk, K., Baldi, P., & Bernard,
862 C. (2020). The circadian dynamics of the hippocampal transcriptome and proteome is altered in
863 experimental temporal lobe epilepsy. *Science Advances*, *6*(41), eaat5979.
864 https://doi.org/10.1126/sciadv.aat5979
865 Donevan, R. E., Anderson, N. M., Sekelj, P., Papp, O., & McGregor, M. (1962). Influence of voluntary
866 hyperventilation on cardiac output. *Journal of Applied Physiology*, *17*(3), 487–491.
867 https://doi.org/10.1152/jappl.1962.17.3.487
868 Edwards, S. B., & de Olmos, J. S. (1976). Autoradiographic studies of the projections of the midbrain
869 reticular formation: Ascending projections of nucleus cuneiformis. *The Journal of Comparative*
870 *Neurology*, *165*(4), 417–431. https://doi.org/10.1002/cne.901650403
871 Eldridge, F. L., Kiley, J. P., & Millhorn, D. E. (1984). Respiratory effects of carbon dioxide-induced changes
872 of medullary extracellular fluid pH in cats. *The Journal of Physiology*, *355*, 177–189.
873 https://doi.org/10.1113/jphysiol.1984.sp015413
874 Ferlisi, M., & Shorvon, S. (2014). Seizure precipitants (triggering factors) in patients with epilepsy.
875 *Epilepsy & Behavior: E&B*, *33*, 101–105. https://doi.org/10.1016/j.yebeh.2014.02.019
876 Festing, M. F. W. (1979). Inbred Strains of Rats. In M. F. W. Festing (Ed.), *Inbred Strains in Biomedical*
877 *Research* (pp. 267–296). Macmillan Education UK. https://doi.org/10.1007/978-1-349-03816-
878 9_14
879 Fountain, N. B., Kim, J. S., & Lee, S. I. (1998). Sleep Deprivation Activates Epileptiform Discharges
880 Independent of the Activating Effects of Sleep. *Journal of Clinical Neurophysiology*, *15*(1), 69–75.
881 Guyenet, P. G. (2014). Regulation of Breathing and Autonomic Outflows by Chemoreceptors.
882 *Comprehensive Physiology*, *4*(4), 1511–1562. https://doi.org/10.1002/cphy.c140004
883 Guyenet, P. G., & Bayliss, D. A. (2015). Neural Control of Breathing and CO2 Homeostasis. *Neuron*, *87*(5),
884 946–961. http://dx.doi.org/10.1016/j.neuron.2015.08.001
885 Guyenet, P. G., Bayliss, D. A., Stornetta, R. L., Ludwig, M.-G., Kumar, N. N., Shi, Y., Burke, P. G. R., Kanbar,
886 R., Basting, T. M., Holloway, B. B., & Wenker, I. C. (2016). Proton detection and breathing
887 regulation by the retrotrapezoid nucleus. *The Journal of Physiology*, *594*(6), 1529–1551.
888 https://doi.org/10.1113/JP271480
889 Guyenet, P. G., Stornetta, R. L., Souza, G. M. P. R., Abbott, S. B. G., Shi, Y., & Bayliss, D. A. (2019). The
890 Retrotrapezoid Nucleus: Central Chemoreceptor and Regulator of Breathing Automaticity.
891 *Trends in Neurosciences*, *42*(11), 807–824. https://doi.org/10.1016/j.tins.2019.09.002
892 Helbig, I. (2015). Genetic Causes of Generalized Epilepsies. *Seminars in Neurology*, *35*(03), 288–292.
893 https://doi.org/10.1055/s-0035-1552922

Herzog, A. G., & Frye, C. A. (2014). Allopregnanolone levels and seizure frequency in progesterone-treated women with epilepsy. *Neurology*, *83*(4), 345–348. https://doi.org/10.1212/WNL.0000000000000623

Holowach, J., Thurston, D., & O'Leary, J. L. (1962). Petit Mal Epilepsy. *Pediatrics*, *30*, 893–901.

Hughes, J. R. (2009). Absence seizures: A review of recent reports with new concepts. *Epilepsy & Behavior*, *15*(4), 404–412. https://doi.org/10.1016/j.yebeh.2009.06.007

Huguenard, J. (2019). Current Controversy: Spikes, Bursts, and Synchrony in Generalized Absence Epilepsy: Unresolved Questions Regarding Thalamocortical Synchrony in Absence Epilepsy. *Epilepsy Currents*, *19*(2), 105–111. https://doi.org/10.1177/1535759719835355

Huguenard, J. R., & McCormick, D. A. (2007). Thalamic synchrony and dynamic regulation of global forebrain oscillations. *Trends in Neurosciences*, *30*(7), 350–356. https://doi.org/10.1016/j.tins.2007.05.007

Hunter, J., & Jasper, H. H. (1949). Effects of thalamic stimulation in unanaesthetised animals: The arrest reaction and petit Mal-like seizures, activation patterns and generalized convulsions. *Electroencephalography and Clinical Neurophysiology*, *1*(1–4), 305–324. http://dx.doi.org/10.1016/0013-4694(49)90196-0

Hwang, D. Y., Carlezon, W. A., Isacson, O., & Kim, K. S. (2001). A high-efficiency synthetic promoter that drives transgene expression selectively in noradrenergic neurons. *Human Gene Therapy*, *12*(14), 1731–1740. https://doi.org/10.1089/104303401750476230

Jasper, H. H., & Droogleever-Fortuyn, J. (1947). Experimental studies of the functional anatomy of petit mal epilepsy. *Res. Publ. Assoc. Res. Nerve Ment. Dis.*, *26*, 272–298.

Joshi, S., & Kapur, J. (2019). Neurosteroid regulation of GABAA receptors: A role in catamenial epilepsy. *Brain Research*, *1703*, 31–40. https://doi.org/10.1016/j.brainres.2018.02.031

Kasteleijn-Nolst Trenité, D. G. A. (2012). Provoked and reflex seizures: Surprising or common? *Epilepsia*, *53 Suppl 4*, 105–113. https://doi.org/10.1111/j.1528-1167.2012.03620.x

Koeleman, B. P. C. (2018). What do genetic studies tell us about the heritable basis of common epilepsy? Polygenic or complex epilepsy? *Neuroscience Letters*, *667*, 10–16. https://doi.org/10.1016/j.neulet.2017.03.042

Koepp, M. J., Caciagli, L., Pressler, R. M., Lehnertz, K., & Beniczky, S. (2016). Reflex seizures, traits, and epilepsies: From physiology to pathology. *The Lancet. Neurology*, *15*(1), 92–105. https://doi.org/10.1016/S1474-4422(15)00219-7

Laffey, J. G., & Kavanagh, B. P. (2002). Hypocapnia. *New England Journal of Medicine*, *347*(1), 43–53. https://doi.org/10.1056/NEJMra012457

Lein, E. S., Hawrylycz, M. J., Ao, N., Ayres, M., Bensinger, A., Bernard, A., Boe, A. F., Boguski, M. S., Brockway, K. S., Byrnes, E. J., Chen, L., Chen, L., Chen, T.-M., Chi Chin, M., Chong, J., Crook, B. E., Czaplinska, A., Dang, C. N., Datta, S., … Jones, A. R. (2007). Genome-wide atlas of gene expression in the adult mouse brain. *Nature*, *445*(7124), 168–176. https://doi.org/10.1038/nature05453

Lennox, W. G. (1928). The effect on epileptic seizures of varying composition of respired air. *J. Clin. Investigation*, *6*, 23–24.

Lindsey, B. G., Nuding, S. C., Segers, L. S., & Morris, K. F. (2018). Carotid Bodies and the Integrated Cardiorespiratory Response to Hypoxia. *Physiology*, *33*(4), 281–297. https://doi.org/10.1152/physiol.00014.2018

Lonergan, T., Teschemacher, A. G., Hwang, D. Y., Kim, K.-S., Pickering, A. E., & Kasparov, S. (2005). Targeting brain stem centers of cardiovascular control using adenoviral vectors: Impact of promoters on transgene expression. *Physiological Genomics*, *20*(2), 165–172. https://doi.org/10.1152/physiolgenomics.00120.2004

López-Barneo, J., Macías, D., Platero-Luengo, A., Ortega-Sáenz, P., & Pardal, R. (2016). Carotid body oxygen sensing and adaptation to hypoxia. *Pflugers Archiv: European Journal of Physiology*, *468*(1), 59–70. https://doi.org/10.1007/s00424-015-1734-0

Lum, L. M., Connolly, M. B., Farrell, K., & Wong, P. K. H. (2002). Hyperventilation-induced High-amplitude Rhythmic Slowing with Altered Awareness: A Video-EEG Comparison with Absence Seizures. *Epilepsia (Series 4)*, *43*(11), 1372–1378. https://doi.org/10.1046/j.1528-1157.2002.35101.x

Lusardi, T. A., Akula, K. K., Coffman, S. Q., Ruskin, D. N., Masino, S. A., & Boison, D. (2015). Ketogenic diet prevents epileptogenesis and disease progression in adult mice and rats. *Neuropharmacology*, *99*, 500–509. http://dx.doi.org/10.1016/j.neuropharm.2015.08.007

Ma, X., Zhang, Y., Yang, Z., Liu, X., Sun, H., Qin, J., Wu, X., & Liang, J. (2011). Childhood absence epilepsy: Electroclinical features and diagnostic criteria. *Brain and Development*, *33*(2), 114–119. http://dx.doi.org/10.1016/j.braindev.2010.02.004

Malow, B. A., Selwa, L. M., Ross, D., & Aldrich, M. S. (1999). Lateralizing value of interictal spikes on overnight sleep-EEG studies in temporal lobe epilepsy. *Epilepsia*, *40*(11), 1587–1592. https://doi.org/10.1111/j.1528-1157.1999.tb02044.x

Masino, S. A., Kawamura Jr, M., Ruskin, D. N., Geiger, J. D., & Boison, D. (2012). Purines and neuronal excitability: Links to the ketogenic diet. *Epilepsy Research*, *100*(3), 229–238. http://dx.doi.org/10.1016/j.eplepsyres.2011.07.014

Masino, S. A., & Rho, J. M. (2012). Mechanisms of Ketogenic Diet Action. In J. L. Noebels, M. Avoli, M. A. Rogawski, R. W. Olsen, & A. V. Delgado-Escueta (Eds.), *Jasper's Basic Mechanisms of the Epilepsies* (4th ed.). National Center for Biotechnology Information (US). http://www.ncbi.nlm.nih.gov/books/NBK98219/

Masino, S. A., & Rho, J. M. (2019). Metabolism and epilepsy: Ketogenic diets as a homeostatic link. *Brain Research*, *1703*, 26–30. https://doi.org/10.1016/j.brainres.2018.05.049

Mattozzi, S., Cerminara, C., Sotgiu, M. A., Carta, A., Coniglio, A., Roberto, D., Simula, D. M., Luca Pruneddu, G., Dell'Avvento, S., Muzzu, S. S., Fadda, M., Luzzu, G. M., Sotgiu, S., & Casellato, S. (2021). Occurrence of hyperventilation-induced high amplitude rhythmic slowing with altered awareness after successful treatment of typical absence seizures and a network hypothesis. *Clinical Neurophysiology Practice*, *6*, 185–188. https://doi.org/10.1016/j.cnp.2021.03.009

McCafferty, C., David, F., Venzi, M., Lőrincz, M. L., Delicata, F., Atherton, Z., Recchia, G., Orban, G., Lambert, R. C., Di Giovanni, G., Leresche, N., & Crunelli, V. (2018). Cortical drive and thalamic feed-forward inhibition control thalamic output synchrony during absence seizures. *Nature Neuroscience*, *21*(5), 744–756. https://doi.org/10.1038/s41593-018-0130-4

McCormick, D. A., & Contreras, D. (2001). On The Cellular and Network Bases of Epileptic Seizures. *Annual Review of Physiology*, *63*(1), 815–846. https://doi.org/10.1146/annurev.physiol.63.1.815

Meeren, H. K. M., Pijn, J. P. M., Van Luijtelaar, E. L. J. M., Coenen, A. M. L., & Lopes da Silva, F. H. (2002). Cortical Focus Drives Widespread Corticothalamic Networks during Spontaneous Absence Seizures in Rats. *The Journal of Neuroscience*, *22*(4), 1480–1495.

Meeren, H., van Luijtelaar, G., Lopes da Silva, F., & Coenen, A. (2005). Evolving concepts on the pathophysiology of absence seizures: The cortical focus theory. *Archives of Neurology*, *62*(3), 371–376. https://doi.org/10.1001/archneur.62.3.371

Meuth, S. G., Budde, T., Kanyshkova, T., Broicher, T., Munsch, T., & Pape, H.-C. (2003). Contribution of TWIK-Related Acid-Sensitive K+ Channel 1 (TASK1) and TASK3 Channels to the Control of Activity Modes in Thalamocortical Neurons. *The Journal of Neuroscience*, *23*(16), 6460–6469.

Meuth, S. G., Kanyshkova, T., Meuth, P., Landgraf, P., Munsch, T., Ludwig, A., Hofmann, F., Pape, H.-C., & Budde, T. (2006). Membrane Resting Potential of Thalamocortical Relay Neurons Is Shaped by

the Interaction Among TASK3 and HCN2 Channels. *Journal of Neurophysiology*, *96*(3), 1517–1529. https://doi.org/10.1152/jn.01212.2005

Nobili, L., Baglietto, M. G., Beelke, M., De Carli, F., Veneselli, E., & Ferrillo, F. (2001). Temporal relationship of generalized epileptiform discharges to spindle frequency activity in childhood absence epilepsy. *Clinical Neurophysiology: Official Journal of the International Federation of Clinical Neurophysiology*, *112*(10), 1912–1916. https://doi.org/10.1016/s1388-2457(01)00624-1

Padmanaban, V., Inati, S., Ksendzovsky, A., & Zaghloul, K. (2019). Clinical advances in photosensitive epilepsy. *Brain Research*, *1703*, 18–25. https://doi.org/10.1016/j.brainres.2018.07.025

Paxinos, G., & Watson, C. (2007). *The Rat Brain In Sterotaxic Coordinates* (6th ed.). Elsevier.

Paz, J. T., & Huguenard, J. R. (2015). Microcircuits and their interactions in epilepsy: Is the focus out of focus? *Nat Neurosci*, *18*(3), 351–359. https://doi.org/10.1038/nn.3950

Pinault, D. (2003). Cellular interactions in the rat somatosensory thalamocortical system during normal and epileptic 5–9 Hz oscillations. *The Journal of Physiology*, *552*(3), 881–905. https://doi.org/10.1113/jphysiol.2003.046573

Pinault, D., Leresche, N., Charpier, S., Deniau, J.-M., Marescaux, C., Vergnes, M., & Crunelli, V. (1998). Intracellular recordings in thalamic neurones during spontaneous spike and wave discharges in rats with absence epilepsy. *The Journal of Physiology*, *509*(2), 449–456. https://doi.org/10.1111/j.1469-7793.1998.449bn.x

Raichle, M. E., & Plum, F. (1972). Hyperventilation and Cerebral Blood Flow. *Stroke*, *3*(5), 566–575. https://doi.org/10.1161/01.STR.3.5.566

Reddy, D. S., Kim, H.-Y., & Rogawski, M. A. (2001). Neurosteroid Withdrawal Model of Perimenstrual Catamenial Epilepsy. *Epilepsia*, *42*(3), 328–336. https://doi.org/10.1046/j.1528-1157.2001.10100.x

Robinson, P. F., & Gilmore, S. A. (1980). Spontaneous generalized spike-wave discharges in the electrocorticograms of albino rats. *Brain Research*, *201*(2), 452–458. https://doi.org/10.1016/0006-8993(80)91052-5

Robinson, R., Taske, N., Sander, T., Heils, A., Whitehouse, W., Goutières, F., Aicardi, J., Lehesjoki, A.-E., Siren, A., Laue Friis, M., Kjeldsen, M. J., Panayiotopoulos, C., Kennedy, C., Ferrie, C., Rees, M., & Gardiner, R. M. (2002). Linkage analysis between childhood absence epilepsy and genes encoding GABAA and GABAB receptors, voltage-dependent calcium channels, and the ECA1 region on chromosome 8q. *Epilepsy Research*, *48*(3), 169–179. https://doi.org/10.1016/S0920-1211(01)00335-7

Ropert, N., & Steriade, M. (1981). Input-output organization of midbrain reticular core. *Journal of Neurophysiology*, *46*(1), 17–31. https://doi.org/10.1152/jn.1981.46.1.17

Russo, E., Citraro, R., Constanti, A., Leo, A., Lüttjohann, A., van Luijtelaar, G., & De Sarro, G. (2016). Upholding WAG/Rij rats as a model of absence epileptogenesis: Hidden mechanisms and a new theory on seizure development. *Neuroscience & Biobehavioral Reviews*, *71*, 388–408. https://doi.org/10.1016/j.neubiorev.2016.09.017

Saalmann, Y. B. (2014). Intralaminar and medial thalamic influence on cortical synchrony, information transmission and cognition. *Frontiers in Systems Neuroscience*, *8*. https://doi.org/10.3389/fnsys.2014.00083

Sadleir, L. G., Farrell, K., Smith, S., Connolly, M. B., & Scheffer, I. E. (2006). Electroclinical features of absence seizures in childhood absence epilepsy. *Neurology*, *67*(3), 413. https://doi.org/10.1212/01.wnl.0000228257.60184.82

Sadleir, L. G., Scheffer, I., Smith, S., Carstensen, B., Farrell, K., & Connolly, M. B. (2009). EEG features of absence seizures in idiopathic generalized epilepsy: Impact of syndrome, age, and state. *Epilepsia*, *50*(6), 1572–1578. https://doi.org/10.1111/j.1528-1167.2008.02001.x

1035 Sander, T., Toliat, M. R., Heils, A., Leschik, G., Becker, C., Rüschendorf, F., Rohde, K., Mundlos, S., &
1036 Nürnberg, P. (2002). Association of the 867Asp variant of the human anion exchanger 3 gene
1037 with common subtypes of idiopathic generalized epilepsy. *Epilepsy Research*, *51*(3), 249–255.
1038 https://doi.org/10.1016/S0920-1211(02)00152-3
1039 Sarrigiannis, P. G., Zhao, Y., He, F., Billings, S. A., Baster, K., Rittey, C., Yianni, J., Zis, P., Wei, H.,
1040 Hadjivassiliou, M., & Grünewald, R. (2018). The cortical focus in childhood absence epilepsy;
1041 evidence from nonlinear analysis of scalp EEG recordings. *Clinical Neurophysiology*, *129*(3), 602–
1042 617. https://doi.org/10.1016/j.clinph.2017.11.029
1043 Semenza, G. L., & Prabhakar, N. R. (2018). The role of hypoxia-inducible factors in carotid body (patho)
1044 physiology. *The Journal of Physiology*, *596*(15), 2977–2983. https://doi.org/10.1113/JP275696
1045 Sherwin, I. (1965). Differential effects of hyperventillation on the excitability of intact and isolated
1046 cortex. *Electroencephalography and Clinical Neurophysiology*, *18*(6), 599–607.
1047 https://doi.org/10.1016/0013-4694(65)90077-5
1048 Sherwin, I. (1967). Alterations in the non-specific cortical afference during hyperventilation.
1049 *Electroencephalography and Clinical Neurophysiology*, *23*(6), 532–538.
1050 https://doi.org/10.1016/0013-4694(67)90019-3
1051 Sinning, A., & Hübner, C. A. (2013). Minireview: PH and synaptic transmission. *FEBS Letters*, *587*(13),
1052 1923–1928. https://doi.org/10.1016/j.febslet.2013.04.045
1053 Sinning, A., Liebmann, L., Kougioumtzes, A., Westermann, M., Bruehl, C., & Hubner, C. A. (2011).
1054 Synaptic Glutamate Release Is Modulated by the Na+-Driven Cl-/HCOFormula Exchanger Slc4a8.
1055 *Journal of Neuroscience*, *31*(20), 7300–7311. https://doi.org/10.1523/JNEUROSCI.0269-11.2011
1056 Smith, J. C., Abdala, A. P. L., Borgmann, A., Rybak, I. A., & Paton, J. F. R. (2013). Brainstem respiratory
1057 networks: Building blocks and microcircuits. *Trends in Neurosciences*, *36*(3), 152–162.
1058 https://doi.org/10.1016/j.tins.2012.11.004
1059 Smyk, M. K., & van Luijtelaar, G. (2020). Circadian Rhythms and Epilepsy: A Suitable Case for Absence
1060 Epilepsy. *Frontiers in Neurology*, *11*. https://doi.org/10.3389/fneur.2020.00245
1061 Souza, G. M. P. R., Kanbar, R., Stornetta, D. S., Abbott, S. B. G., Stornetta, R. L., & Guyenet, P. G. (2018).
1062 Breathing regulation and blood gas homeostasis after near complete lesions of the
1063 retrotrapezoid nucleus in adult rats. *The Journal of Physiology*, *596*(13), 2521–2545.
1064 https://doi.org/10.1113/JP275866
1065 Souza, G. M. P. R., Stornetta, R. L., Stornetta, D. S., Abbott, S. B. G., & Guyenet, P. G. (2019). Contribution
1066 of the Retrotrapezoid Nucleus and Carotid Bodies to Hypercapnia- and Hypoxia-induced Arousal
1067 from Sleep. *The Journal of Neuroscience: The Official Journal of the Society for Neuroscience*,
1068 *39*(49), 9725–9737. https://doi.org/10.1523/JNEUROSCI.1268-19.2019
1069 Souza, G. M. P. R., Stornetta, R. L., Stornetta, D. S., Abbott, S. B. G., & Guyenet, P. G. (2020). Differential
1070 Contribution of the Retrotrapezoid Nucleus and C1 Neurons to Active Expiration and Arousal in
1071 Rats. *The Journal of Neuroscience: The Official Journal of the Society for Neuroscience*, *40*(45),
1072 8683–8697. https://doi.org/10.1523/JNEUROSCI.1006-20.2020
1073 Steriade, M., & Glenn, L. L. (1982). Neocortical and caudate projections of intralaminar thalamic neurons
1074 and their synaptic excitation from midbrain reticular core. *Journal of Neurophysiology*, *48*(2),
1075 352–371. https://doi.org/10.1152/jn.1982.48.2.352
1076 Stirling, R. E., Cook, M. J., Grayden, D. B., & Karoly, P. J. (2021). Seizure forecasting and cyclic control of
1077 seizures. *Epilepsia*, *62*(S1), S2–S14. https://doi.org/10.1111/epi.16541
1078 Taylor, J. A., Reuter, J. D., Kubiak, R. A., Mufford, T. T., Booth, C. J., Dudek, F. E., & Barth, D. S. (2019).
1079 Spontaneous Recurrent Absence Seizure-like Events in Wild-Caught Rats. *Journal of*
1080 *Neuroscience*, *39*(24), 4829–4841. https://doi.org/10.1523/JNEUROSCI.1167-18.2019

Taylor, J. A., Rodgers, K. M., Bercum, F. M., Booth, C. J., Dudek, F. E., & Barth, D. S. (2017). Voluntary Control of Epileptiform Spike–Wave Discharges in Awake Rats. *The Journal of Neuroscience*, *37*(24), 5861–5869. https://doi.org/10.1523/JNEUROSCI.3235-16.2017

Ting, J. T., Daigle, T. L., Chen, Q., & Feng, G. (2014). Acute Brain Slice Methods for Adult and Aging Animals: Application of Targeted Patch Clamp Analysis and Optogenetics. In M. Martina & S. Taverna (Eds.), *Patch-Clamp Methods and Protocols* (pp. 221–242). Springer New York. https://doi.org/10.1007/978-1-4939-1096-0_14

Tyvaert, L., Chassagnon, S., Sadikot, A., LeVan, P., Dubeau, F., & Gotman, J. (2009). Thalamic nuclei activity in idiopathic generalized epilepsy: An EEG-fMRI study. *Neurology*, *73*(23), 2018–2022. https://doi.org/10.1212/WNL.0b013e3181c55d02

van Luijtelaar, E. L., & Coenen, A. M. (1986). Two types of electrocortical paroxysms in an inbred strain of rats. *Neuroscience Letters*, *70*(3), 393–397.

Vergnes, M., Marescaux, Ch., Micheletti, G., Reis, J., Depaulis, A., Rumbach, L., & Warter, J. M. (1982). Spontaneous paroxysmal electroclinical patterns in rat: A model of generalized non-convulsive epilepsy. *Neuroscience Letters*, *33*(1), 97–101. https://doi.org/10.1016/0304-3940(82)90136-7

von Krosigk, M., Bal, T., & McCormick, D. (1993). Cellular mechanisms of a synchronized oscillation in the thalamus. *Science*, *261*(5119), 361. https://doi.org/10.1126/science.8392750

Watemberg, N., Farkash, M., Har-Gil, M., Sezer, T., Goldberg-Stern, H., & Alehan, F. (2015). Hyperventilation During Routine Electroencephalography: Are Three Minutes Really Necessary? *Pediatric Neurology*, *52*(4), 410–413. http://dx.doi.org/10.1016/j.pediatrneurol.2014.12.003

Xie, H., Su, W., Pei, J., Zhang, Y., Gao, K., Li, J., Ma, X., Zhang, Y., Wu, X., & Jiang, Y. (2019). De novo SCN1A, SCN8A, and CLCN2 mutations in childhood absence epilepsy. *Epilepsy Research*, *154*, 55–61. https://doi.org/10.1016/j.eplepsyres.2019.04.005

Yang, X.-F., Shi, X.-Y., Ju, J., Zhang, W.-N., Liu, Y.-J., Li, X.-Y., & Zou, L.-P. (2014). 5% CO2 inhalation suppresses hyperventilation-induced absence seizures in children. *Epilepsy Research*, *108*(2), 345–348. http://dx.doi.org/10.1016/j.eplepsyres.2013.11.012

Table 1. Spike-wave seizure count.

Figure	Comparison	Bin Count (Mean ± S.E.)	n	p value
1D	Normoxia Hypoxia	0.89 ± 0.12 1.73 ± 0.13	15	4.5×10^{-3}
3C	Normoxia Hypoxia	0.99 ± 0.18 1.82 ± 0.14	9	1.76×10^{-6}
3F	Normoxia Hypoxia + CO_2	1.09 ± 0.22 0.84 ± 0.13	9	0.18
4C	Normoxia Normoxia + CO_2	1.36 ± 0.17 0.95 ± 0.10	8	0.0028
5D	Normoxia Normoxia + Photostim.	1.17 ± 0.38 2.27 ± 0.63	10	0.002
5G	Normoxia Normoxia + Photostim.+ CO_2	1.04 ± 0.32 1.01 ± 0.30	6	0.86

Table 2. Respiratory Rate.

Figure	Comparison	Resp. Rate (Hz) (Mean ± S.E.)	n	p value
1E	Normoxia Hypoxia	1.03 ± 0.02 1.33 ± 0.05	15	1.67×10^{-5}
3D	Normoxia Hypoxia	1.00 ± 0.02 1.28 ± 0.05	9	6.59×10^{-6}
3G	Normoxia Hypoxia + CO_2	1.06 ± 0.03 1.88 ± 0.15	9	2.71×10^{-4}
4D	Normoxia Normoxia + CO_2	0.99 ± 0.03 1.78 ± 0.10	9	3.78×10^{-5}
5E	Normoxia Normoxia + Photostim.	1.02 ± 0.03 1.24 ± 0.08	10	0.019
5H	Normoxia Normoxia + Photostim.+ CO_2	1.01 ± 0.03 1.84 ± 0.08	6	0.031

Table 3. Arterial measurements in Wistar rats.

Figure	Parameter	Comparison	Value	n	p value
2C1	PaO2	Normoxia Hypoxia	83.25 ± 2.32 32.25 ± 1.25	4	0.0002
2C2	PaCO2	Normoxia Hypoxia	37.0 ± 0.59 22.33 ± 0.16	4	6.6×10^{-5}
2C3	pH	Normoxia Hypoxia	7.47 ± 0.01 7.63 ± 0.01	4	4.5×10^{-5}

Table 4. Arterial measurements in WAG/Rij rats.

Figure	Parameter	Comparison	Value	n	p value
3H1	PaO_2	Normoxia Hypoxia	84.93 ± 1.82 34.50 ± 0.56	6	6.0×10^{-6}
		Normoxia Hypoxia +CO_2	84.93 ± 0.02 55.83 ± 0.87	6	0.000134
3H2	$PaCO_2$	Normoxia Hypoxia	43.48 ± 0.47 25.83 ± 0.65	6	2.1×10^{-6}
		Normoxia Hypoxia +CO_2	43.48 ± 0.47 44.60 ± 0.55	6	0.42
3H3	pH	Normoxia Hypoxia	7.45 ± 0.01 7.61 ± 0.01	6	7.0×10^{-6}
		Normoxia Hypoxia +CO_2	7.45 ± 0.01 7.43 ± 0.01	6	0.008
4E1	PaO_2	Normoxia 5% CO2	84.93 ± 1.82 34.50 ± 0.56	6	0.00019
4E2	$PaCO_2$	Normoxia 5% CO2	43.48 ± 0.47 25.83 ± 0.65	6	0.022
4E3	pH	Normoxia 5% CO2	7.45 ± 0.01 7.42 ± 0.01	6	0.00063

Table 5. cFos-positive cells in WAG/Rij rats.

Figure	Threshold	Comparison	Counts (Mean ± S.E.)	n	p value
6C	3	Normoxia Hypoxia	282 ± 148.2 1370 ± 137	4	1.5×10^{-7}
		Normoxia Hypoxia + CO2	282 ± 148.2 385.5 ± 78.7	4	0.55
		Hypoxia Hypoxia + CO2	1370 ± 137 385.5 ± 78.7	4	4.3×10^{-7}
	5	Normoxia Hypoxia	112.3 ± 57.1 595.3 ± 85.0	4	0.0005
		Normoxia Hypoxia + CO2	112.3 ± 57.1 348 ± 68.9	4	0.045
		Hypoxia Hypoxia + CO2	595.3 ± 85.0 348 ± 68.9	4	0.061
	7	Normoxia Hypoxia	57.3 ± 29.2 349 ± 75.0	4	0.021
		Normoxia Hypoxia + CO2	57.3 ± 29.2 319.5 ± 63.1	4	0.036
		Hypoxia Hypoxia + CO2	349 ± 75.0 319.5 ± 63.1	4	0.95